Novel microbend loss fiber optic hydrophones for direction sensing

by

Ashish M. Vengsarkar

Thesis submitted to the Faculty of the

Virginia Polytechnic Institute and State University

in partial fulfillment of the requirements for the degree of

Master of Science

in

Electrical Engineering

APPROVED:

Richard O. Claus, Chairman

Ahmad Safaai-Jazi

Ronald G. Pieper

August, 1988

Blacksburg, Virginia

Novel microbend loss fiber optic hydrophones for direction sensing

by

Ashish M. Vengsarkar

Richard O. Claus, Chairman

Electrical Engineering

(ABSTRACT)

Dual purpose fiber optic microbend loss sensors have been developed for measurement of underwater acoustic wave amplitudes and for detection of the direction of wave propagation. Cylindrical sensing elements with external threads have fibers wound around them. Axial slots, cut along the length of the cylinder and deeper than the threads, provide the microbends. Three different construction schemes for cylindrical sensing elements are built. The dual purpose hydrophones are characterized for frequencies ranging from 15 kHz to 75 kHz. Based on the results, an improved design that uses the wavelength dependence of microbend loss in a single mode fiber is proposed.

Acknowledgements

I wish to thank Dr. Richard O. Claus, my advisor, for his guidance and constant words of encouragement, and Dr. Ahmad Safaai-Jazi and Dr. Ronald J. Pieper, for useful discussions and for serving on my graduate committee.

I am extremely grateful to who spent many hours working on this project, patiently assuring me that the idea would work, and for his assistance, specially with the electronics. Some of the best ideas presented in this thesis belong to them.

Many thanks to all my fellow researchers, and and for making work a pleasure at FEORC.

Finally, I would like to take this opportunity to thank Dr. B. V. Rao of the Indian Institute of Technology, Bombay, for introducing me to the area of fiber optic sensing.

Table of Contents

List of Illustrations

1.0 INTRODUCTION

Microbends are repititive changes in the radius of curvature of an optical fiber which result in a decrease in the transmitted optical power. The increase in attenuation is due to repititive coupling of energy between the guided modes or between the guided and the leaky modes of an optical fiber. Such a loss induced by microbends has long been considered a bane by designers of optical communication systems. The same mechanism, on the other hand, has been put to advantage in fiber optic sensors for the detection of external perturbations such as pressure, vibration, displacement and strain [1,2].

A simple microbend loss sensor system consists of a multimode fiber placed between two grooved plates with a spatial period Λ. An external disturbance, which is the parameter to be sensed, physically displaces the plates leading to an introduction of microbends, which causes mode coupling. This mode coupling redistributes the light among core modes and also couples light from core to clad modes. Monitoring the light power associated with either core or clad modes

determines the amplitude of the disturbance. Such intensity modulated sensors have the attraction of optical simplicity; however, drawbacks include lower sensitivities compared to phase modulated schemes and complex structures of the sensing elements.

One specific application that is considered here is the detection of underwater acoustic waves. Microbend loss sensors for detection of pressure have been widely investigated in the literature [3,4,5,6] and sensitivities in the range of - 200 dB re 1V/μPa have been obtained for underwater sensing. Most of the sensors have been used for amplitude detection and the problem of detecting the direction has been left unaddressed. A need is therefore felt to explore new fiber optic sensing schemes for the detection of both the amplitude and the direction of an underwater acoustic source. This project sets out to do just that.

Chapter 2 serves as an introduction to the theory of microbend losses in optical fibers and to the parameters that determine sensitivity and overall system performance. It also includes a discussion of the wavelength dependence of microbend losses in single mode fibers. Three novel sensing schemes are presented in Chapter 3. All designs use multimode fibers. The mechanism of operation is described for each sensing element and the possible drawbacks are considered. Results obtained from experiments are presented in Chapter 4. Obvious drawbacks and deviations from expected results lead us to suggestions for improvements in system performance. An improved wavelength dependent microbend loss scheme is proposed in Chapter 5. This includes ramifications of

the theory presented in Chapter 2 and specific details of an experimental set-up that uses a spectral attenuation measurement system. Chapter 6 includes a summary of work done, conclusions drawn and suggestions for future work.

2.0 THEORY

In this chapter, we present the theoretical background on which the design of the hydrophones is based. System considerations are first discussed with an emphasis on those parameters that determine system sensitivity and efficiency. The theory of microbend loss is divided into two different sections based on the type of fiber used - multimode or single mode. From this discussion, it will be observed that the microbend loss in single mode fibers shows a different behavior for different wavelengths of light. This dependence will be considered in the last section.

2.1 System considerations

A schematic of a microbend loss sensing system is shown in Figure 1.

Let P_{in} be the optical power incident into the fiber at the input end and P_{out} be the optical power at the output of the fiber, which is incident on the photodetector. If T is the transmission coefficient for the modes travelling in the fiber, then,

$$P_{out} = P_{in} \cdot T \ . \tag{2.1.1}$$

When an acoustic pressure ΔP is incident on the loss modulator, the transmission coefficient changes by ΔT and the detector signal current is given by [4]

$$i_s = \left(\frac{qeP_{in}}{h\nu} \right) \left(\frac{\Delta T}{\Delta P} \right) \ \Delta P \, , \tag{2.1.2}$$

where q is the quantum efficiency of the detector, h is Planck's constant, ν is the light frequency and ΔT/ΔP is the transduction coefficient of the sensor.

The mean-square shot noise current in the detector is given by [7]

$$i_n^2 = 2e \left(\frac{qe}{h\nu} \right) \ P_{in} \, T \, \Delta f \tag{2.1.3}$$

where Δf is the detection bandwidth. The signal to noise ratio (SNR) can be obtained from (2.1.2) and (2.1.3).

$$SNR = \frac{i_s^2}{i_n^2} = \frac{1}{2T\Delta f} \frac{qP_{in}}{h\nu} \left(\frac{\Delta T}{\Delta P} \right)^2 (\Delta P)^2 \qquad (2.1.4)$$

The minimum detectable pressure, assuming a shot-noise limited sensor and equating the SNR to 1 is

$$P_{\min} = \left(\frac{2Th\nu\Delta f}{qP_{in}} \right)^{1/2} \left(\frac{\Delta T}{\Delta P} \right)^{-1}. \qquad (2.1.5)$$

When the power in the core modes is monitored, the transmission coefficient T can vary typically from 0.1 to 1. When the power in the cladding modes is monitored, however, T can be several orders of magnitude smaller, since these modes can be easily stripped just before the sensing element [6]. Thus, dark field detection allows, in principle, the detection of significantly smaller pressure fields.

We now focus on the transduction coefficient of the sensor ($\Delta T/\Delta P$), which can be written as

$$\frac{\Delta T}{\Delta P} = \left(\frac{\Delta T}{\Delta x} \right) \left(\frac{\Delta x}{\Delta P} \right), \qquad (2.1.6)$$

where Δx is the change in the amplitude of the fiber deformation. ($\Delta T/\Delta x$) depends on the sensitivity of the optical fiber to microbending losses and ($\Delta x/\Delta P$) depends on the acoustical and mechanical design of the sensor. We have thus managed to separate the optical and mechanical properties of the sensor that have a bearing on the transduction coefficient and hence the system performance.

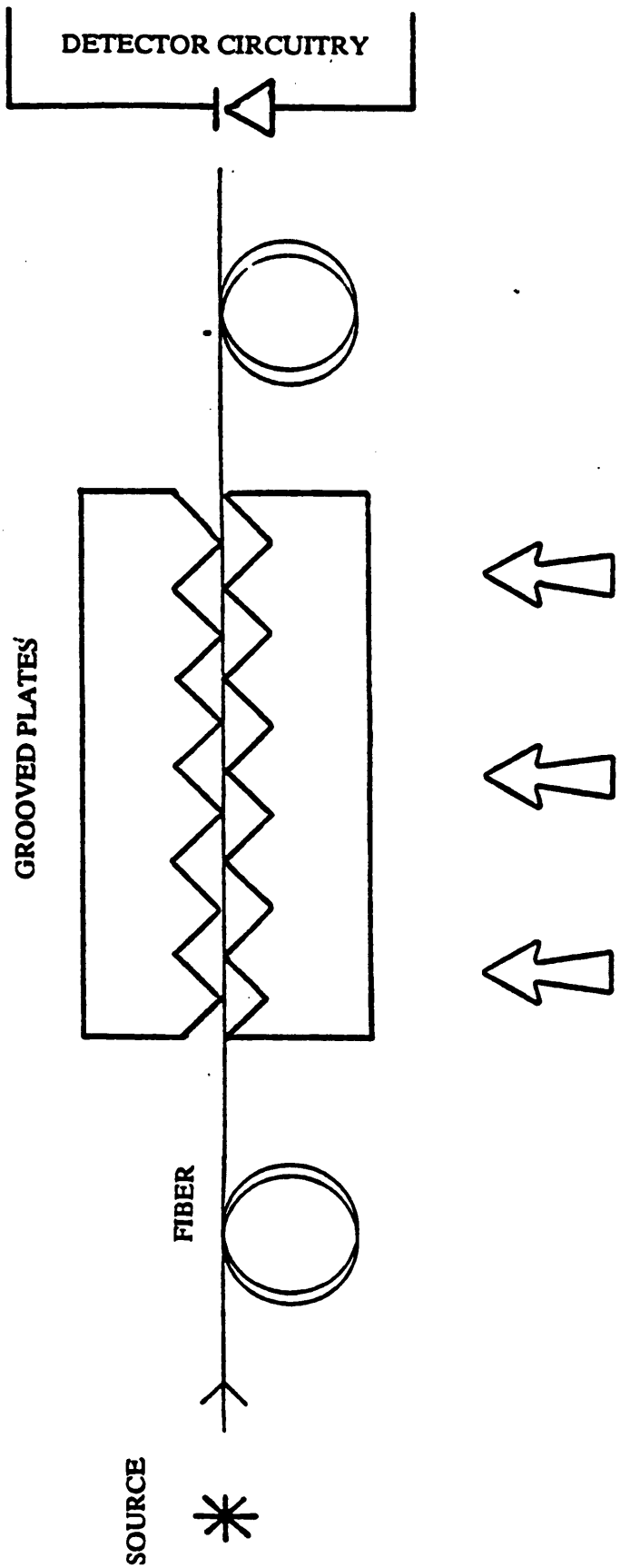

Figure 1. Typical microbend loss sensing system

2.2 Optical parameters

We first look at the optical part of the transduction coefficient. It can be shown [8,9] that power coupling between two modes with propagation constants k and k' is maximum when

$$k - k' = \pm \frac{2\pi}{\Lambda} , \tag{2.2.1}$$

where Λ is the mechanical wavelength of periodic perturbation. It has also been shown [10,11] that the WKB approximation gives the relation

$$k_{m+1} - k_m = \left(\frac{\alpha}{\alpha+2}\right)^2 \frac{2\sqrt{\Delta}}{a} \left(\frac{m}{M}\right)^{[\alpha-2/\alpha+2]} , \tag{2.2.2}$$

where α is the refractive index profile constant, m is the mode label, M is the total number of guided modes and $\Delta = [n^2(0) - n^2(a)]/2n^2(0)$. Equating (2.2.1) and (2.2.2) for step-index fibers ($\alpha = \infty$), we get

$$\Lambda = \frac{\pi a}{\sqrt{\Delta}} \left(\frac{M}{m}\right) . \tag{2.2.3}$$

Equation (2.2.3) implies that higher order modes are coupled for smaller Λs while lower order modes are coupled for higher Λs. Maximum coupling would take place when the highest order guided mode coupled all its power to the radiation modes. This gives us the critical mechanical wavelength Λ_c , for $m = M$,

$$\Lambda_c = \frac{\pi a}{\sqrt{\Delta}} \ . \qquad (2.2.4)$$

For a parabolic index fiber ($\alpha = 2$), we get

$$\Lambda = \frac{2\pi a}{\sqrt{2\Delta}} \ . \qquad (2.2.5)$$

Equation (2.2.5) shows that, in a parabolic index fiber, all modes are equally spaced in k space and hence this Λ couples all adjacent modes equally efficiently.

2.3 Mechanical parameters

In the last section, we have seen how the choice of Λ determines which modes in a multimode fiber couple power. Given those constraints, we would immediately choose Λ_c, for a step-index fiber, as the desired spatial period so as to achieve maximum power transfer between the highest order guided mode and radiation modes. There is, however, a trade-off between the optical and mechanical parameters that finally determines the transduction coefficient.

Consider the mechanical part of the transduction coefficient given in (2.1.6), $\Delta x/\Delta P$, which can be written as [3]

$$\frac{\Delta x}{\Delta P} = AC_m, \tag{2.3.1}$$

where A is the area of the acoustic coupler against which the pressure is applied and C_m is the mechanical compliance of the sensor. It is obvious that the mechanical design of the sensor determines $\Delta x/\Delta P$. Since the exact mechanical design to be used in the experiments that follow is not yet known, we will consider an example [3] shown in Figure 2.

The rubber sleeve in Figure 2 is the acoustic coupler and may not be used in the experiments. The equivalent acoustic circuit is shown in Figure 3.

P is the applied pressure, C_{A_1} and C_{A_2} are the acoustic compliances of the exposed and the unexposed portions of the fiber, C_{A_r} is the acoustic compliance of the rubber tube, M_{A_1} and M_{A_2} are the acoustic masses of the exposed and unexposed portions of the fiber, and M_r is the effective acoustic mass of the rubber tube plus a radiation reactance mass.

We are now interested in finding C_m in (2.3.1), so as to find $\Delta x/\Delta P$. When the compliance of the surrounding fluid is substantially larger than the mechanical compliance of the sensor C_f, the compliance of the sensor C_m is approximately equal to C_f.

$$C_m \simeq C_f. \tag{2.3.2}$$

The mechanical compliance of the sensor over one periodic interval is given by C'_f,

$$C'_f = \frac{C_f}{n}. \tag{2.3.3}$$

C'_f is further related to the effective acoustic compliance C'_A of the sensor by

$$C'_f = \frac{C'_A}{A'^2}, \tag{2.3.4}$$

where A' is the area of the acoustic coupler per periodic interval.

From Figure 3, the effective acoustic compliance C'_A of the sensor per periodic interval can be expressed as follows:

$$\frac{1}{C'_A} = \frac{1}{C_{A_1}} + \frac{1}{C_{A_2}} + \frac{1}{C_r} \,. \tag{2.3.5}$$

In most practical cases the compliance of the acoustic coupler is much larger than that of the bent fiber and can be ignored. We also assume that fiber deflections in the exposed and unexposed section are equal and hence,

$$C_{A_1} = C_{A_2} \,. \tag{2.3.6}$$

Equation (2.3.5) can be written as

$$C'_A = \frac{C_{A_1}}{2} \,. \tag{2.3.7}$$

The effective acoustic compliance per periodic interval C'_A can be shown to be [12]

$$C'_A = G \frac{\Lambda^3}{Ed^4} A'^2 \,, \tag{2.3.8}$$

where G is a constant which depends on how the fiber is loaded and suspended.

Equations (2.3.1) - (2.3.8) give us the desired relation between the mechanical part of the transduction coefficient and physically measurable parameters, from which

$$\frac{\Delta x}{\Delta P} = G \frac{\Lambda^3}{Ed^4} \frac{A}{n} . \tag{2.3.9}$$

The resonance of the sensor ω_o is determined from the following equation:

$$\omega_o^2 = \frac{1}{M_A C'_A} , \tag{2.3.10}$$

where,

$$M_A = M_{A_1} + M_{A_2} + M_{A_r} ,$$

as shown in Figure 3.

We see from equation (2.2.1) that for maximum coupling needed for optimizing optical sensitivity, Λ_c is the smallest of the allowed spatial periods. However, equation (2.3.9) shows that a small Λ reduces the mechanical sensitivity. This is the trade-off that we discussed at the beginning of this section. High sensitivity is obtained with highly compliant fibers. This can be achieved with a large deformer periodicity Λ_c . For large n and d, the Young's modulus E should be small. Also, very small values of d, the fiber diameter, are prevented due to light coupling and fiber mechanical strength considerations. Finally, even though utilizing a small number of deformer intervals n increases $\Delta x/\Delta P$ proportionally,

it decreases $\Delta T/\Delta x$ by the same amount. Thus, the sensor sensitivity is approximately independent of n.

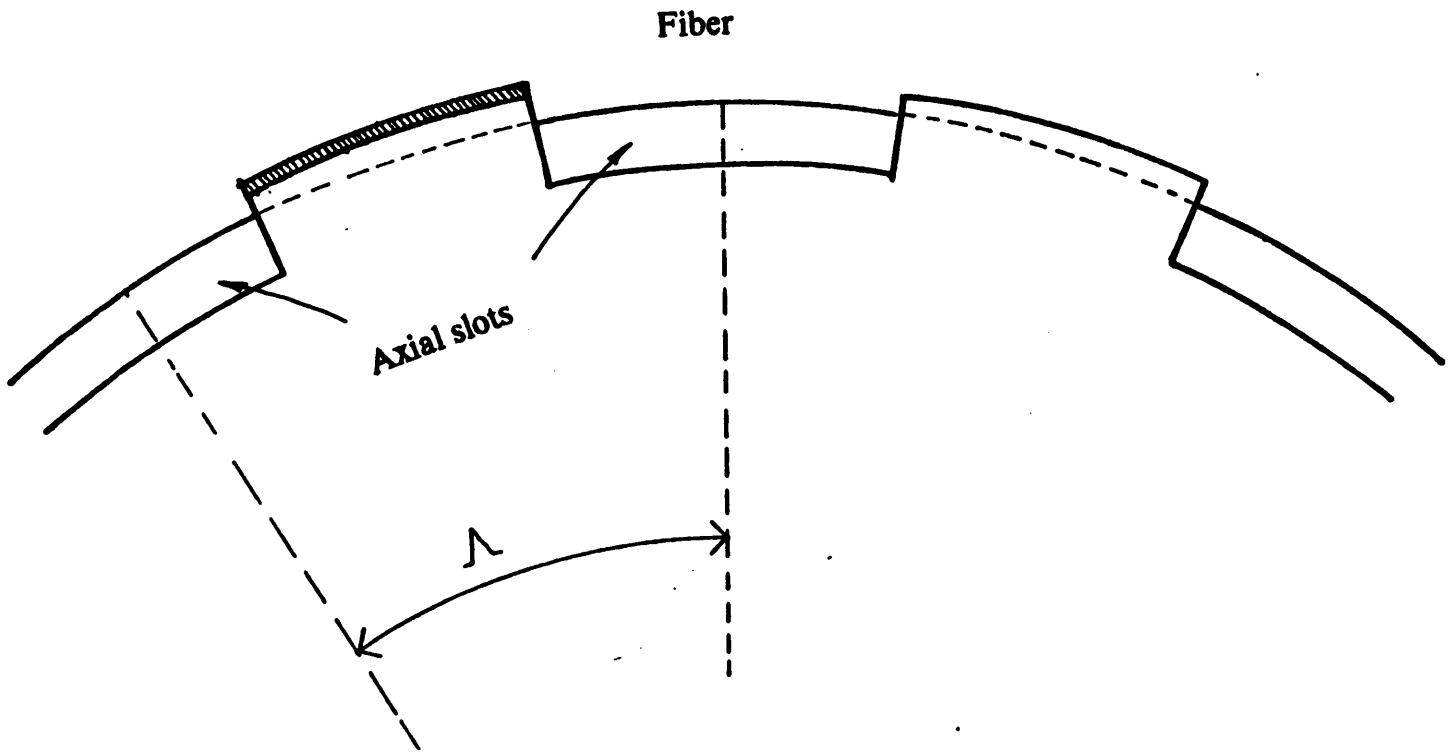

Figure 2. Sensor example for mechanical design considerations

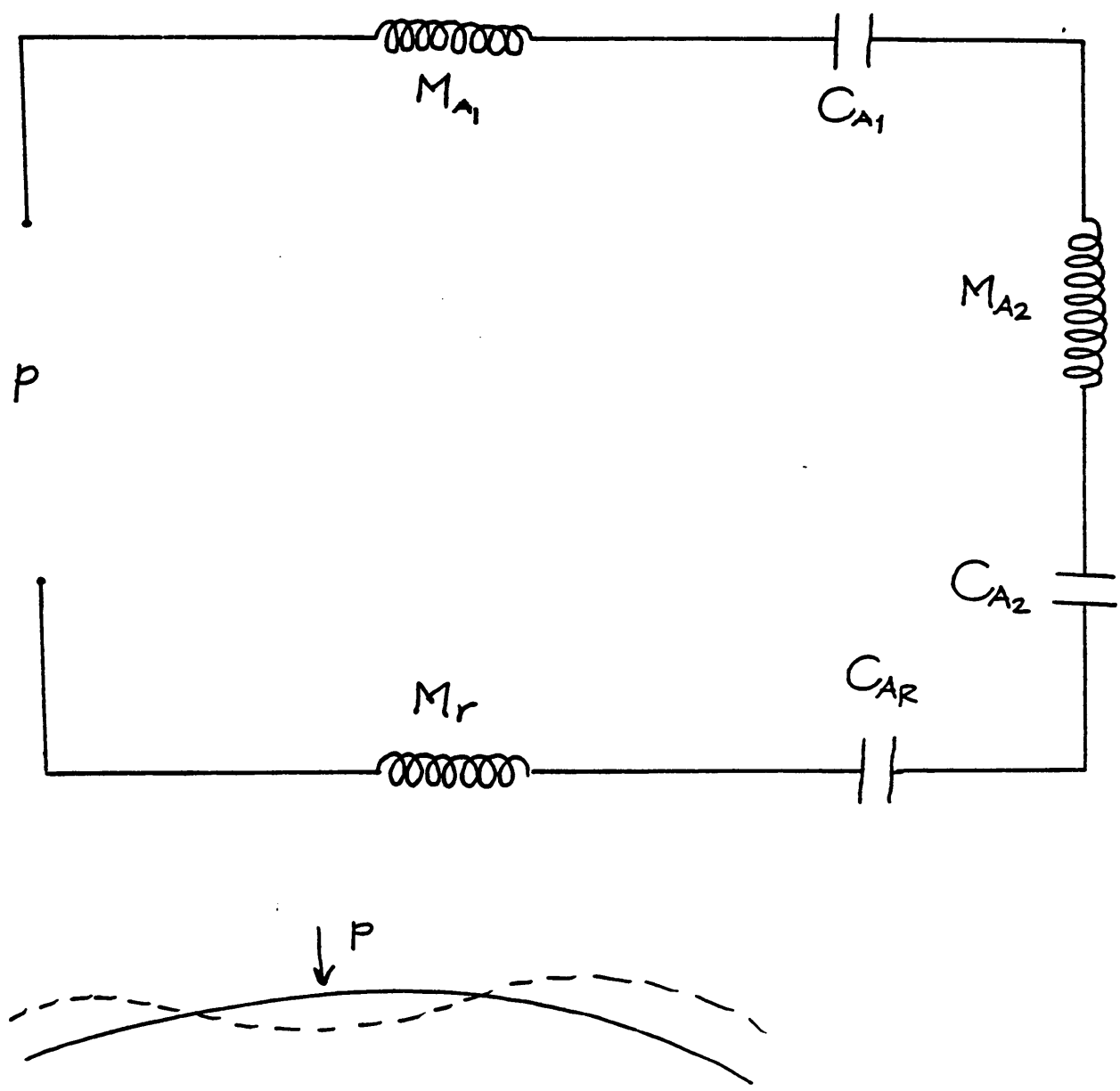

Figure 3. Equivalent acoustic circuit of example in Figure 2

2.4 λ - Dependence of microbend losses in single mode fibers

Microbend loss in multimode fibers has been widely analyzed using the theory developed by Marcuse [13]. This method uses the transverse mode expansion in deformed fibers. Radiation losses have been investigated without considering the direct interaction between guided and radiation modes. It has been assumed that an incident guided mode couples to other guided modes and that the highest order guided mode loses all its power to a radiation wave. In the analysis of microbend losses in single-mode fibers, the direct coupling between guided and radiation waves has to be considered.

The problem of radiation losses in single mode fibers has been investigated in the literature [14-17]. In these analyses, weakly guiding fibers have been studied and only the effect of a fundamental harmonic of deformation spectrum has been considered. We present a method based on the Floquet theory of periodic waveguides [18]. A brief description and the results obtained are given. The reader is referred to Wlodarczyk and Seshadri [19,20] for details.

In the normal mode techniques [13,15], the modes are identified through their transverse dependence using the orthogonality relationship obtained for the unperturbed structure. This approach is particularly attractive for non- periodic perturbations such as tapers or bends. However, periodic perturbations are quite different from non-periodic ones since they give rise to a resonant effect which

are quite different from the modes of an unperturbed waveguide. To formulate the problem, the fields in a periodic fiber are written in the form :

$$E(\rho, \phi, z) = E_o(\rho, \phi, z_o, z_2) + \delta E_1(\rho, \phi, z_o, z_2) + \delta^2 E_2(\rho, \phi, z_o, z_2)\,, \tag{2.4.1a}$$

$$H(\rho, \phi, z) = H_o(\rho, \phi, z_o, z_2) + \delta H_1(\rho, \phi, z_o, z_2) + \delta^2 H_2(\rho, \phi, z_o, z_2)\,, \tag{2.4.1b}$$

where z_0 and z_2 are the fast and slow, respectively, space scales [15] introduced to separate the rapidly and slowly varying fields. Using the chain rule of differentiation $\frac{\partial}{\partial z} = \frac{\partial}{\partial z_0} + \delta \frac{\partial}{\partial z_1} + \delta^2 \frac{\partial}{\partial z_2}$ and the expansions (2.4.1) the following wave equations satisfied by the longitudinal fields E_z and H_z of orders δ^0, δ^1 and δ^2 are obtained.

$$\delta^0\colon\ O_\omega \Psi_{0j}(\rho, \phi, z_0, z_2) = 0 \tag{2.4.2a}$$

$$\delta_1\colon\ O_\omega \Psi_{1j}(\rho, \phi, z_0, z_2) = 0 \tag{2.4.2b}$$

$$\delta^2\colon O_\omega \Psi_{2j}(\rho, \phi, z_0, z_2) = -2 \frac{\partial^2 \Psi_{0j}}{\partial z_0\, \partial z_2} \tag{2.4.2c}$$

where,

$$O_\omega = \frac{\partial^2}{\partial \rho^2} + \frac{1}{\rho}\ \frac{\partial}{\partial \rho} + \frac{1}{\rho^2}\ \frac{\partial^2}{\partial \phi^2} + \frac{\partial^2}{\partial {z_0}^2} + \omega^2 E_r \tag{2.4.2d}$$

and, Ψ_{ij} stands for either E_{iz} ($\Psi_{iE} = E_{iZ}$) or H_{iz} ($\Psi_{iH} = H_{iz}$)

The periodically bent fiber is expressed in a parametric form:

$$[x - \delta x_c(\phi, z)]^2 + [y - \delta y_c(\phi, z)]^2 = a^2 \qquad (2.4.3)$$

where the deformation amplitudes x_c and y_c are assumed to be much smaller than the fiber radius a. In a fashion analogous to the derivation of the equivalent wave equations, (2.4.2), the boundary conditions that must be satisfied by the different orders of δ are then derived. These equivalent boundary conditions at ρ = a can then be solved along with (2.4.2) to give an insight into the behavior of the fields within the periodically perturbed fiber.

Salient results obtained from this approach are:

- The zero-order fields are the fields of a straight, unperturbed fiber. Solution of (2.4.2a) using appropriate boundary conditions leads us to the dispersion relation for hybrid modes in a single mode fiber.

- Solution of the first order fields is useful in obtaining the relationship between the amplitudes of the excited radiation wave and the incident wave. However, this solution does not give information on the effect of mode coupling on the incident wave.

- The solution of the second-order problem describes how the guided mode amplitude and phase change due to the fiber deformation; amplitude and power transport equations are obtained as well.

We are interested in the effect of changing the spatial period Λ and the wavelength of light λ on the microbend losses. In particular, we wish to gain a measure of the microbend loss over a finite length L and analyze dependence of this coefficient on Λ and λ. The radiation loss coefficient τ is given by

$$\tau = \frac{P(L)}{P(0)} = exp(-z \sum_{n}^{N} Re\, q_n L) \qquad (2.4.4)$$

$$= \exp(-zRe\, q_J L)$$

where P(0) and P(L) are the powers in the guided mode at the beginning and end of the perturbation region and $Re\ q_n$ is a leakage factor related to the nth space harmonic.

Figure 4 [20] shows the variation of the real part of q_n with the length of the microbending period Λ for the first three radiation harmonics. The strong wavelength dependence of the losses is shown in Figure 5 [20]. As the source wavelength λ is increased beyond the cutoff value the radiation loss increases dramatically.

Figure 6 [20] shows how the radiation loss varies with Λ for different values of fiber radius a. The critical radius dependence is seen from the increase in the loss for $a = 1.8\lambda$ as compared to $a = 1.7\lambda$. The secondary maxima are suppressed as the fiber approaches the value resulting in maximum loss. It is also noticed that the fiber radius resulting in maximum loss is the same for all harmonics.

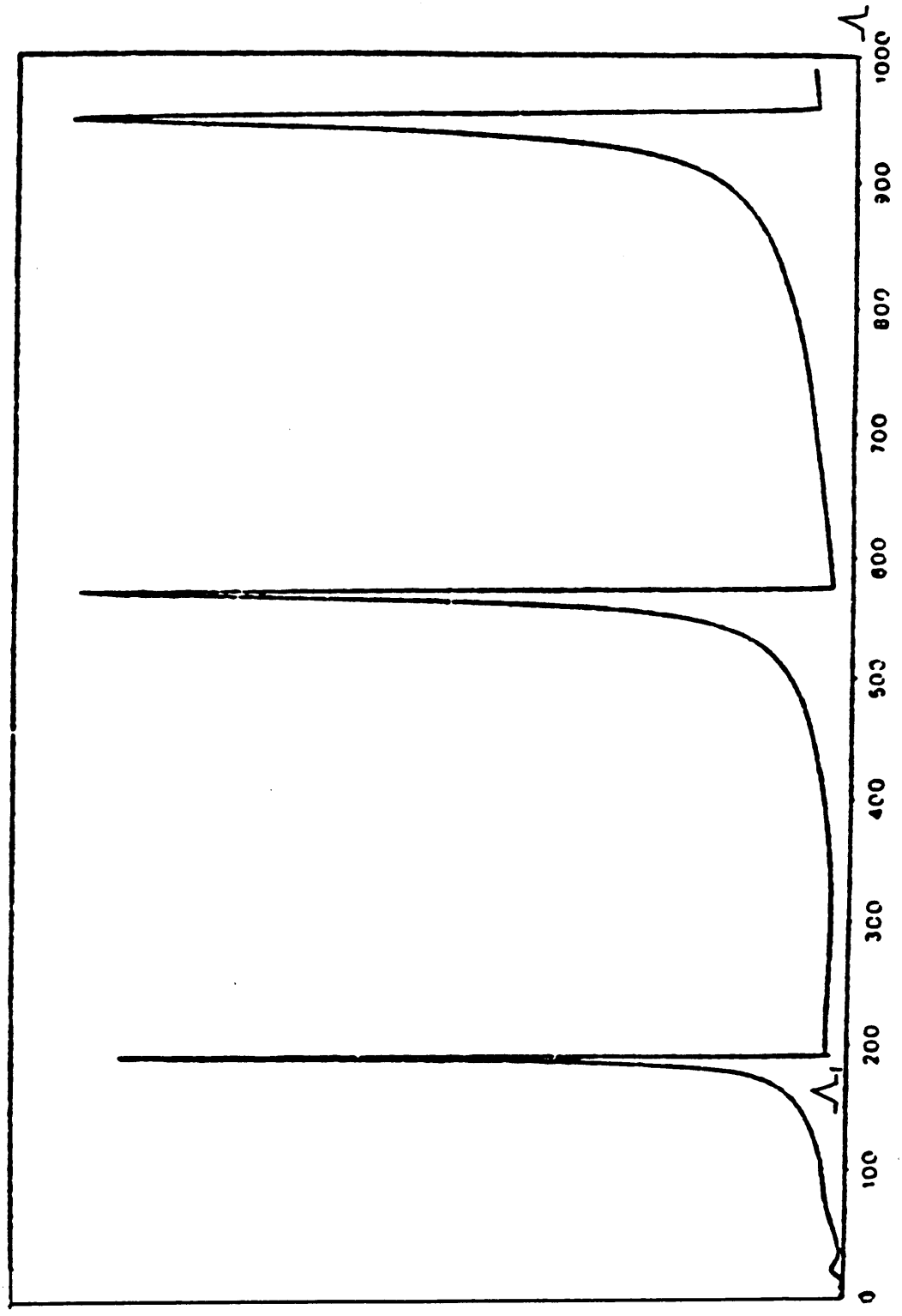

Figure 4. Leakage factor versus Λ for the first three harmonics [20]

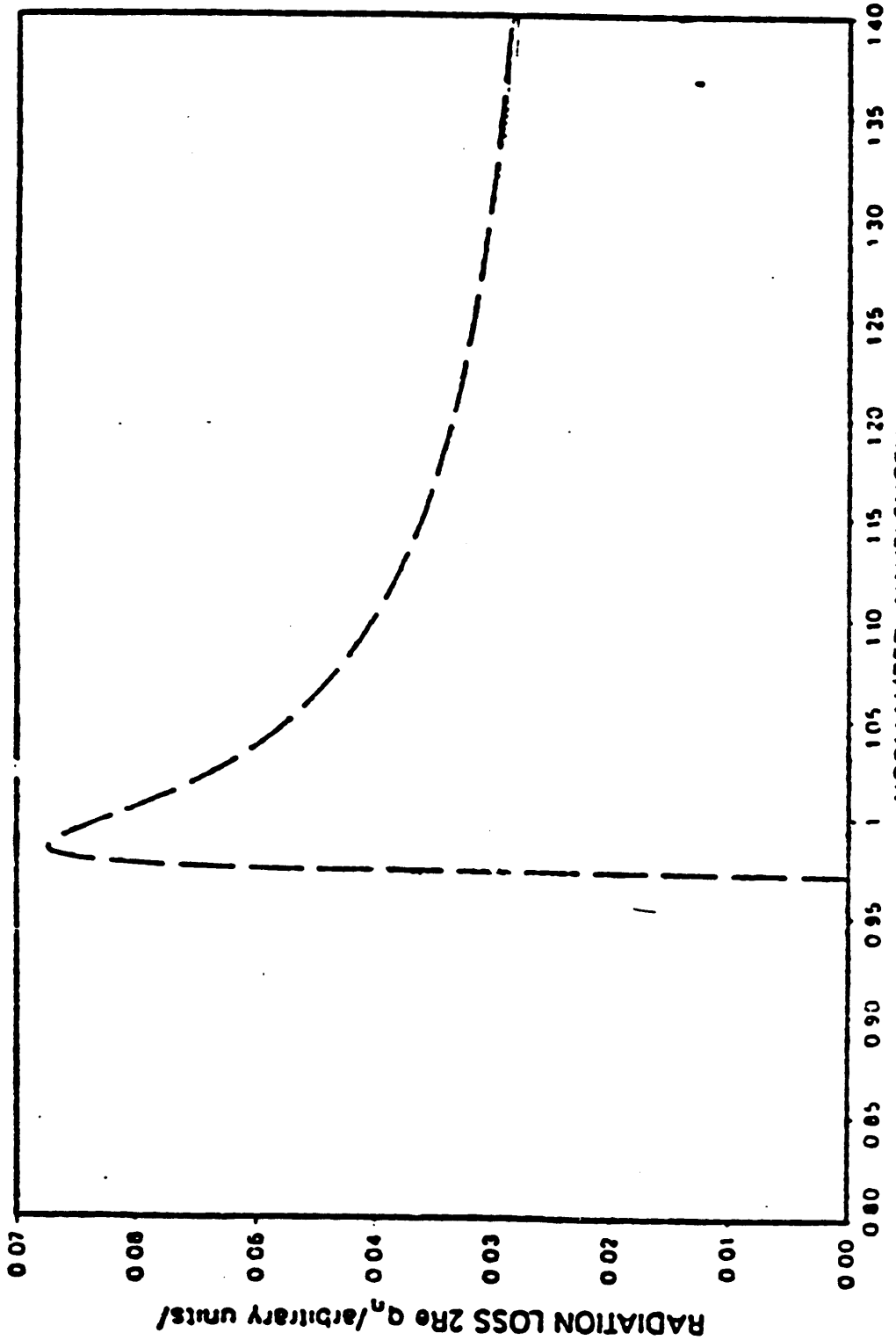

Figure 5. Dependence of microbend loss on λ [20]

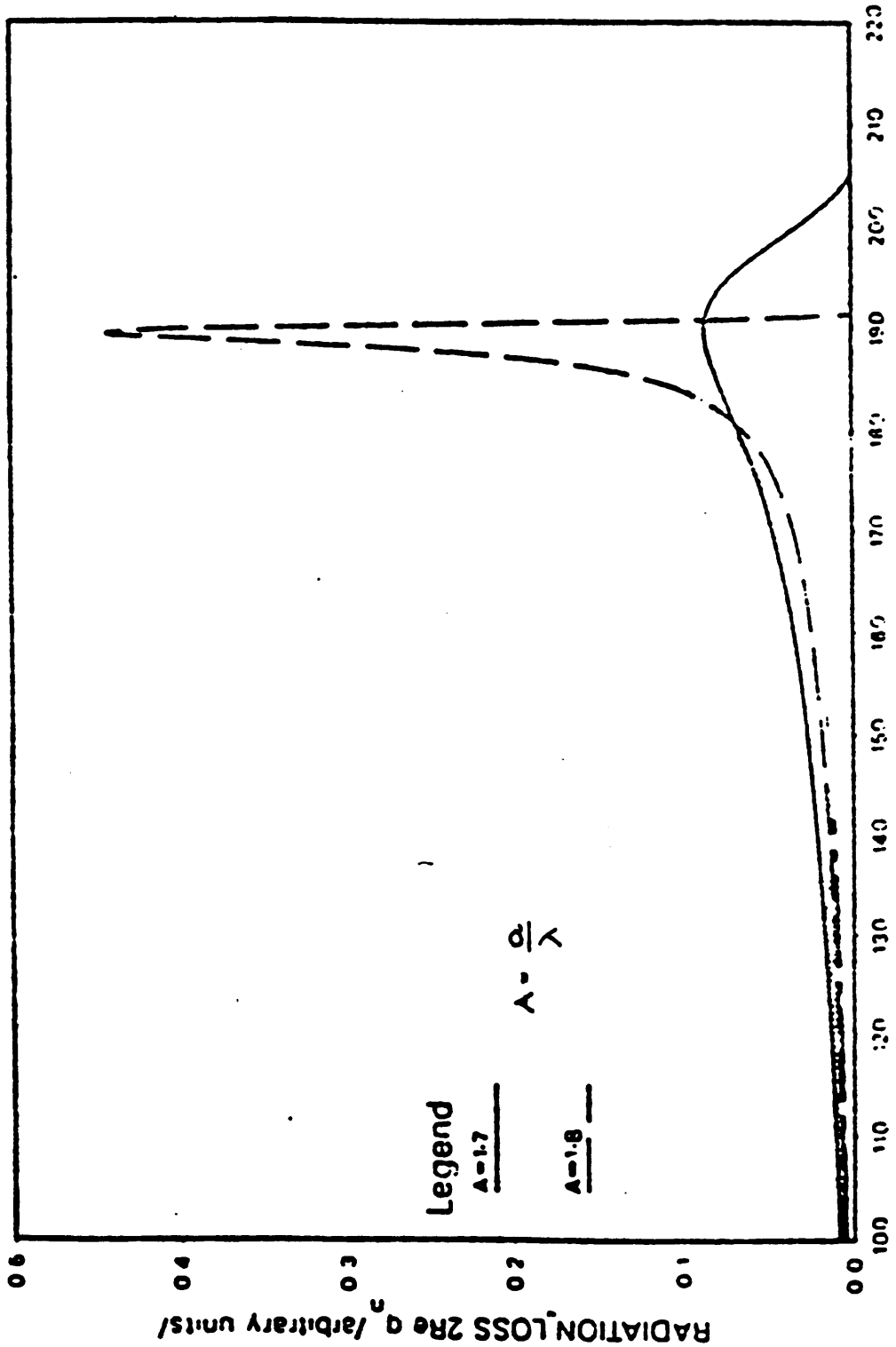

Figure 6. Dependence of microbend loss on Λ and fiber radius [20]

3.0 HYDROPHONE DESIGNS

In most practical cases, microbend losses are induced in fibers with the help of grooved plates. However, applications of sensors using this mechanism are limited to environments where grooved plates cannot be easily installed. The alignment of the grooved plates is critical, the sensor bandwidth is limited and acceleration effects can deteriorate sensor performance. Hence, other geometries need to be considered for underwater applications.

The use of cylindrical sensing elements was first suggested by Lagakos, et al [3]. Some of the advantages of this configuration are mechanical simplicity, acceleration insensitivity and shape flexibility. The designs that we propose and build are variations of the scheme suggested by [3] which detected only the acoustic wave amplitude. The improvisations are aimed towards the detection of the direction of acoustic waves as well.

3.1 Single - fiber fixed Λ rotational (1F/FΛ-R) hydrophone

The design of the sensing element is shown in Figure 7.

Fiber is wound around a cylinder along the external threads machined throughout the length of the cylinder. Axial slots are cut deeper than the external threads and cover only 90 ° of the circumference of the cylinder. The fiber is exposed to the sound field only in the axial slots, since the fiber within the threaded regions and outside the slots does not come in contact with the induced pressure. An incident acoustic wave induces microbends by way of deflections of the fiber within the slots; these microbends result in a reduction in the intensity of the output light. When the pressure wave is incident on region A, as shown in Figure 7, no microbends are induced and the result is an invariance in the output of the fiber. On the other hand, fields incident on the region B will induce some deflection in the fibers and a slight change in the output must be observed. Pressure incident on the region C will induce maximum deflections and hence maximum reduction in power.

Direction sensing can thus be attempted by rotating the cylindrical element. The source can be detected within a ± 45 ° range. Variations of the output power when the source is within the 90 ° arc will have to be monitored experimentally. One of the drawbacks that one can foresee at the designing stage is the

dependence of the readings on the rotation rate of the cylindrical element. Since the noise will be a problem, a certain amount of time may have to be allowed to elapse after each rotation step so as to allow the water to attain a steady state.

A cylindrical sensing element was constructed in the machine shop. The dimensions of the sensor are given below:

External diameter ϕ_o:	50.6 mm
Internal diameter ϕ_i:	19.8 mm
Length l:	60.6 mm
Spatial period Λ:	4.3 mm
External thread pitch:	24 threads/inch
# of axial slots:	10
Total # of microbend interval n:	570
Length of the active fiber:	2442 mm
Mass of the active fiber:	0.8 gram

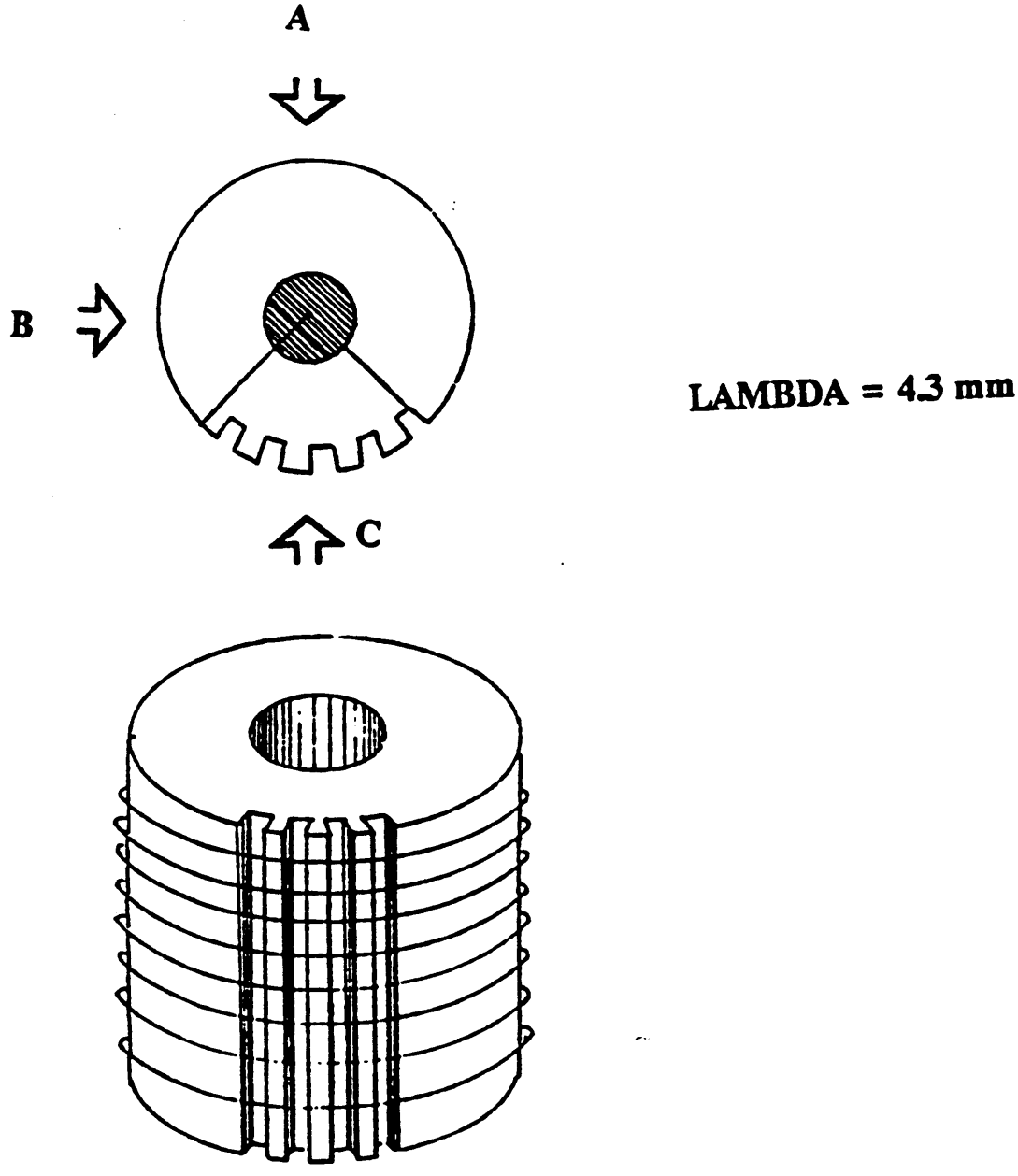

Figure 7. 1F/FΛ-R hydrophone sensing element

3.2 Three - fiber fixed Λ stationary (3F/FΛ-S) hydrophone

A schematic of the 3-fiber stationary hydrophone sensing element is shown in Figure 8. The design is very similar to the single-fiber hydrophone discussed in the previous section. The cylinder is divided into three sections along its length, and the axial slots in each section are disoriented from one another by 90 °. Three different fibers are wound on the sections and the output of each of the fiber segments is monitored.

When the pressure wave is incident on region A, shown in Figure 8, the fiber in section 1 will be deflected and the microbends thus induced will result in a reduction of the output power in fiber wrapped around section 1. Little or no effect will be observed in fibers wrapped around sections 2 and 3. Similarly, fields incident on regions B or C will affect the fiber wrapped around section 2 or 3, respectively. Effects of an acoustic wave impinging on the transition region between sections 1 and 2 or between sections 2 and 3 will have to be monitored experimentally. This design circumvents the problem of rotation that was encountered in the single-fiber hydrophone. However, it adds to the optical complexity of the system by placing the requirement of three detectors for simultaneous monitoring, and by necessitating the use of a 1 × 3 coupler at the input.

A cylindrical sensing element, comprising 3 sections, was constructed along with the single-fiber rotational hydrophone. If each of the three sections were lined up, the sensing element would have a uniform look, as was shown in Figure 7. For the three-fiber sensor, the three sections were rotated 90 ° with respect to one another. The dimensions of the sensor, most values being the same as in the previous design, are given below:

External diameter ϕ_o :	50.6 mm
Internal diameter ϕ_i :	19.8 mm
Lengths l_1, l_2, l_3 :	20.2 mm
Spatial period Λ :	4.3 mm
External thread pitch :	24 threads/inch
# of axial slots :	10
Total # of microbend intervals in each section :	190
Length of active fiber in each section:	814 mm
Mass of active fiber:	0.2 gram

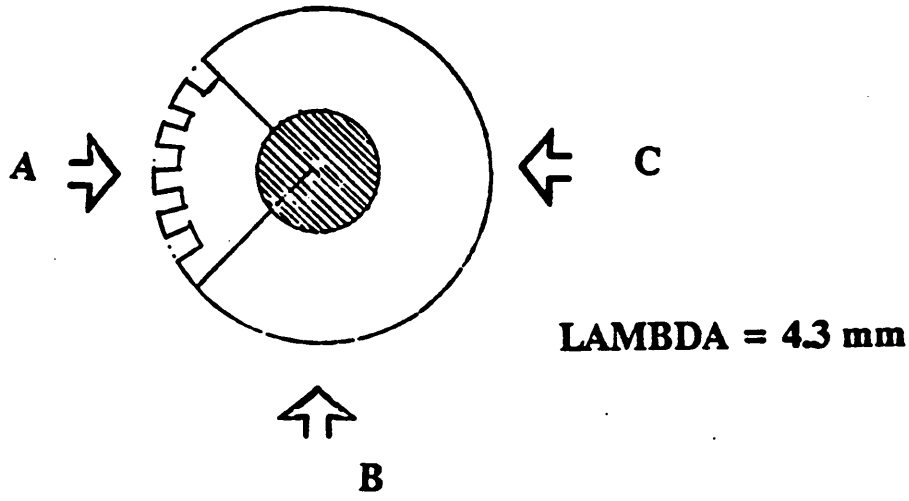

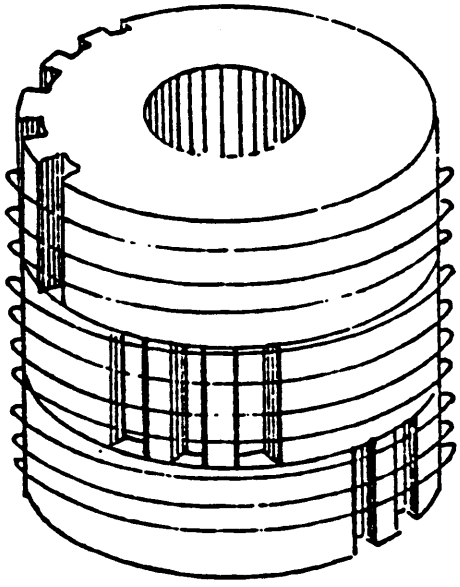

Figure 8. 3F/FΛ-S hydrophone sensing element

3.3 Single-fiber, varying Λ, rotational (1F/VΛ-R) hydrophone

The 1F/FΛ-R hydrophone could have been constructed with an angular arc other than 90 °, the angular arc being the extent of the microbend-inducing axial slots along the circumference. An angle smaller than 90 ° would possibly locate the source with a higher resolution. Under these circumstances, if an acoustic source were present outside the angular arc of axial slots, no signal would be located. Hence, an amplitude measurement of the acoustic signal cannot be performed until the source comes within the arc. If we could construct a sensing element that could measure some amplitude at all times, this problem could possibly be solved. With this in mind, the 1F/VΛ-R fiber-optic hydrophone was designed.

From the equation (2.2.3) we can write

$$\frac{m}{M} = \frac{a\pi}{\sqrt{\Delta}} \quad \frac{1}{\Lambda} ,$$

where m is the mode number, M is the total number of guided modes and other parameters have the standard definitions. This implies that by varying the spatial groove period Λ we should be able to couple a different modal group m to its adjacent mode for a different Λ. Since lower order guided modes propagate closer to the fiber axis, varying Λ along the circumference of the cylindrical sensing

element would lead to different output powers for acoustic waves incidence from different directions. The sensor design is shown in Figure 9.

The dimensions of the sensor are given below:

External diameter ϕ_0 :	50 mm
Internal diameter ϕ_i :	25 mm
Length L :	50 mm
Spatial Period Λ_1 :	4.0 mm
# of slots with spatial period Λ_1, n_1 :	5
Length of active fiber at Λ_1 :	960 mm
Mass of active fiber at Λ_1 :	0.25 gram
Spatial period Λ_2 :	5.2 mm
# of slots with spatial period Λ_2, n_2 :	6
Length of active fiber at Λ_2 :	1498 mm
Mass of active fiber at Λ_2 :	0.4 gram
Spatial period Λ_3 :	6.0 mm
# of slots with spatial period Λ_3, n_3 :	8
Length of active fiber at Λ_3 :	2304 mm
Mass of active fiber at Λ_3 :	0.55 gram
Spatial period Λ_4 :	8.0 mm
# of slots with spatial period Λ_4, n_4 :	6
Length of active fiber at Λ_4 :	2304 mm
Mass of active fiber at Λ_4 :	0.55 gram

External thread pitch : 24 threads/inch

These dimensions and measurements can be used in theoretical calculations, if necessary. Although a theoretical analysis is not presented here, this data will be valuable for future work in this area.

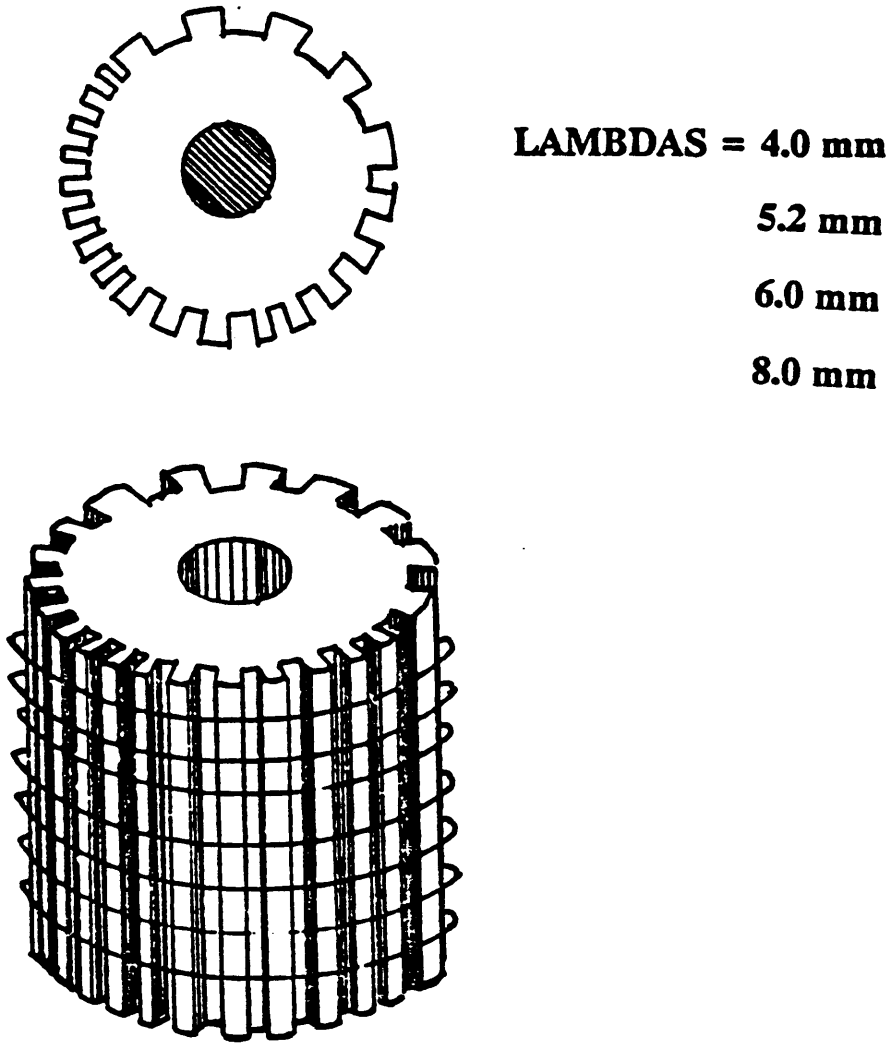

Figure 9. 1F/VΛ-R hydrophone sensing element

4.0 EXPERIMENTS

This chapter describes the characterization of the underwater direction sensors under test conditions. Frequency response in the 15 kHz to 80 kHz range is obtained, input versus output curves are traced, effects of rotating the sensing element or varying Λ are analyzed and, whenever applicable, technical problems associated with the tests are mentioned.

Although methods of data acquisition are explained in detail, the reader is assumed to be familiar with the elementary aspects of fiber optic experimental set-ups.

4.1 Overall description

A schematic diagram of the experimental set-up is shown in Figure 10.

It consists of a He - Ne laser operating at 633 nm, which injects light into a multimode fiber wound around the sensing element. The output of the fiber is spatially filtered before monitoring the power variations with a detector. Spatial filtering is needed because we wish to obtain information about mode-coupling phenomena between modes of specific orders. The detector output is fed into a TEK 7854 oscilloscope, capable of performing several complex mathematical operations on the acquired waveforms. The LeCroy digital oscilloscope is used whenever printed outputs or records are needed.

The water tank is $2' \times 2' \times 2'$ in dimension, made of plexiglass, and houses the underwater acoustic source and the cylindrical sensing element. A Bruel & Kjaer hydrophone (type 8104) is used as the source. The transmitting response of the B&K hydrophones is shown in Figure 11.

The Y axis indicates the transmitted pressure at 1m from the source for a 1V input signal and is given in dB re 1 micropascal. As can be seen, the output is very low for frequencies below 15 kHz and this value puts a limit on the lowest frequency of operation for the system. The optical detector, which was built in the laboratory, determines the higher limit. The frequency response of the detector is

shown in Figure 12. 75 kHz was chosen as the upper frequency of operation in all experiments.

Initial experiments were performed using a continuous wave (cw) operation of the underwater transducer. However, reflections from the walls of the water tank and the water-air interface result in spurious signals. These reflections should be eliminated if accurate direction sensing is to be performed. A pulse wave generated by the circuit was used as an external modulator of the sine wave. A pulsed sine wave was thus acquired and was used as the source for the B&K 8104 hydrophone. Output of the pulse generating circuit and the pulsed sine wave is shown in Figure 13.

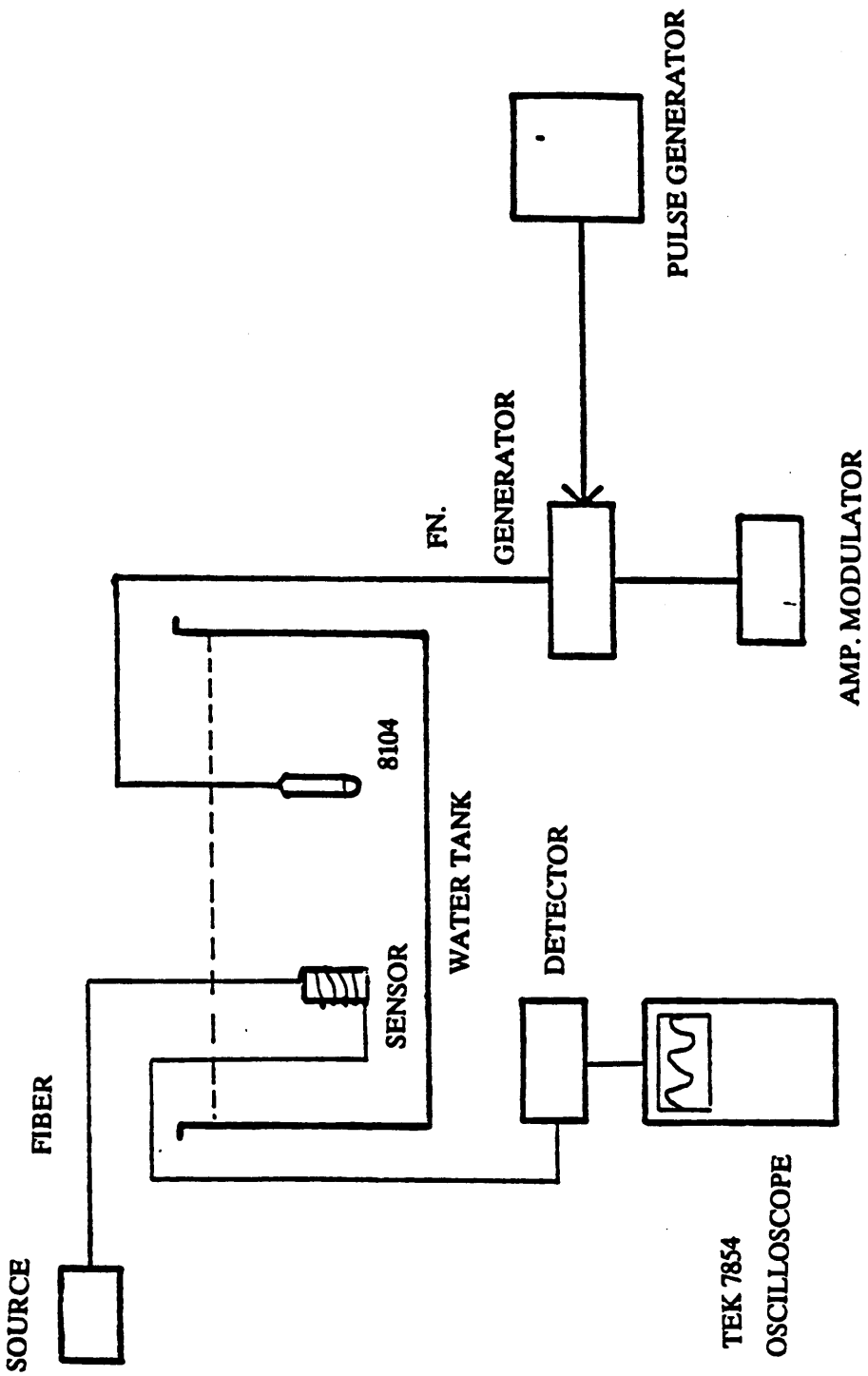

Figure 10. Experimental set-up

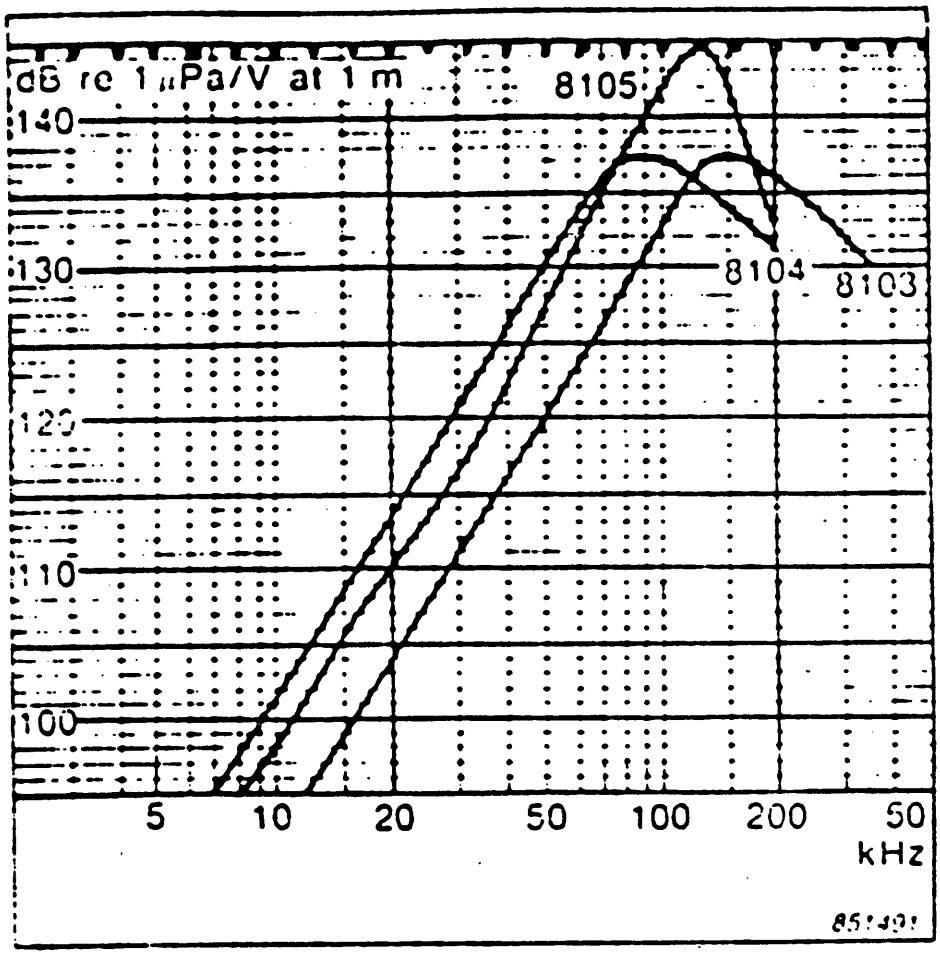

Figure 11. Transmitting response of the B&K hydrophones

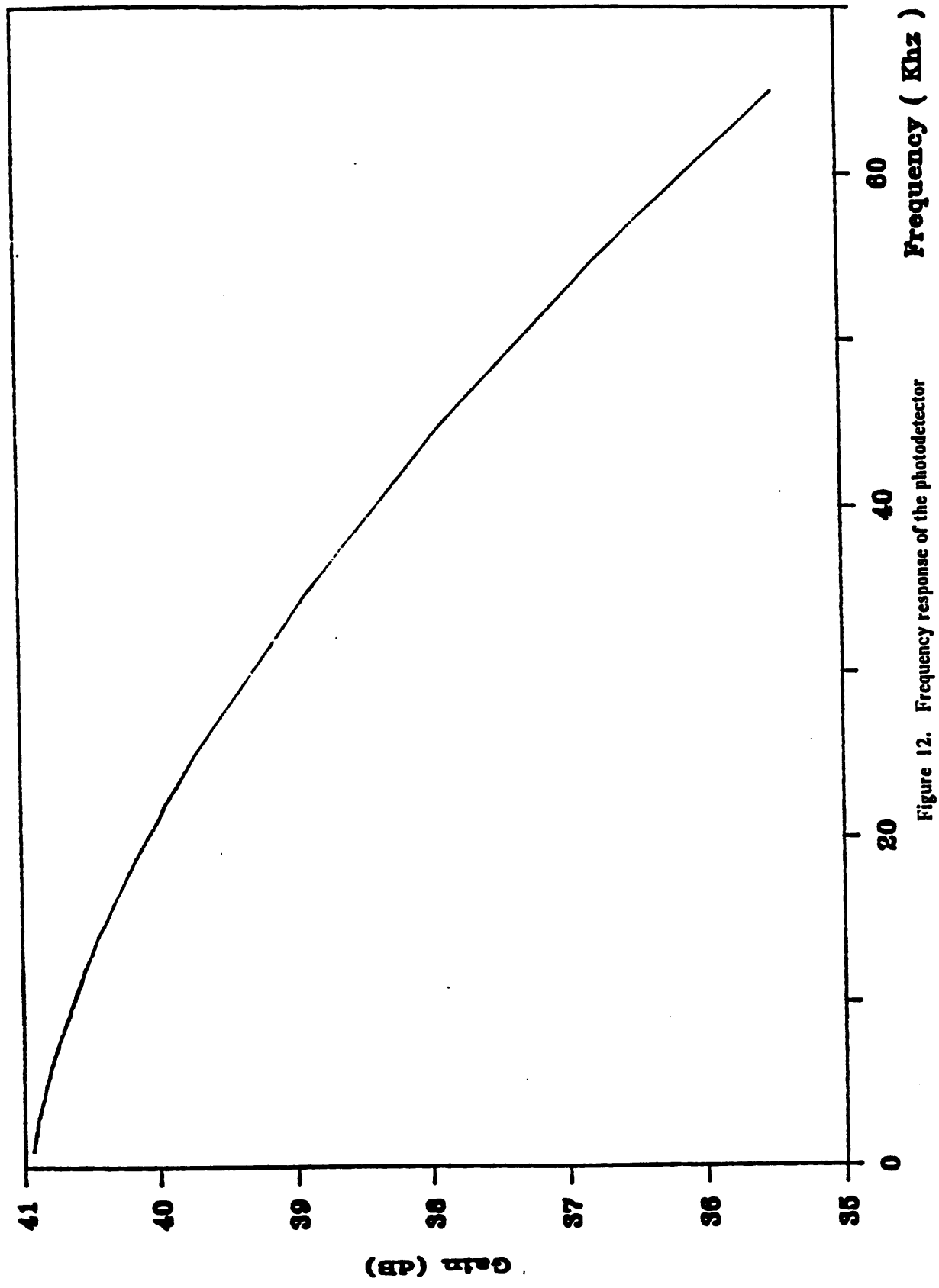

Figure 12. Frequency response of the photodetector

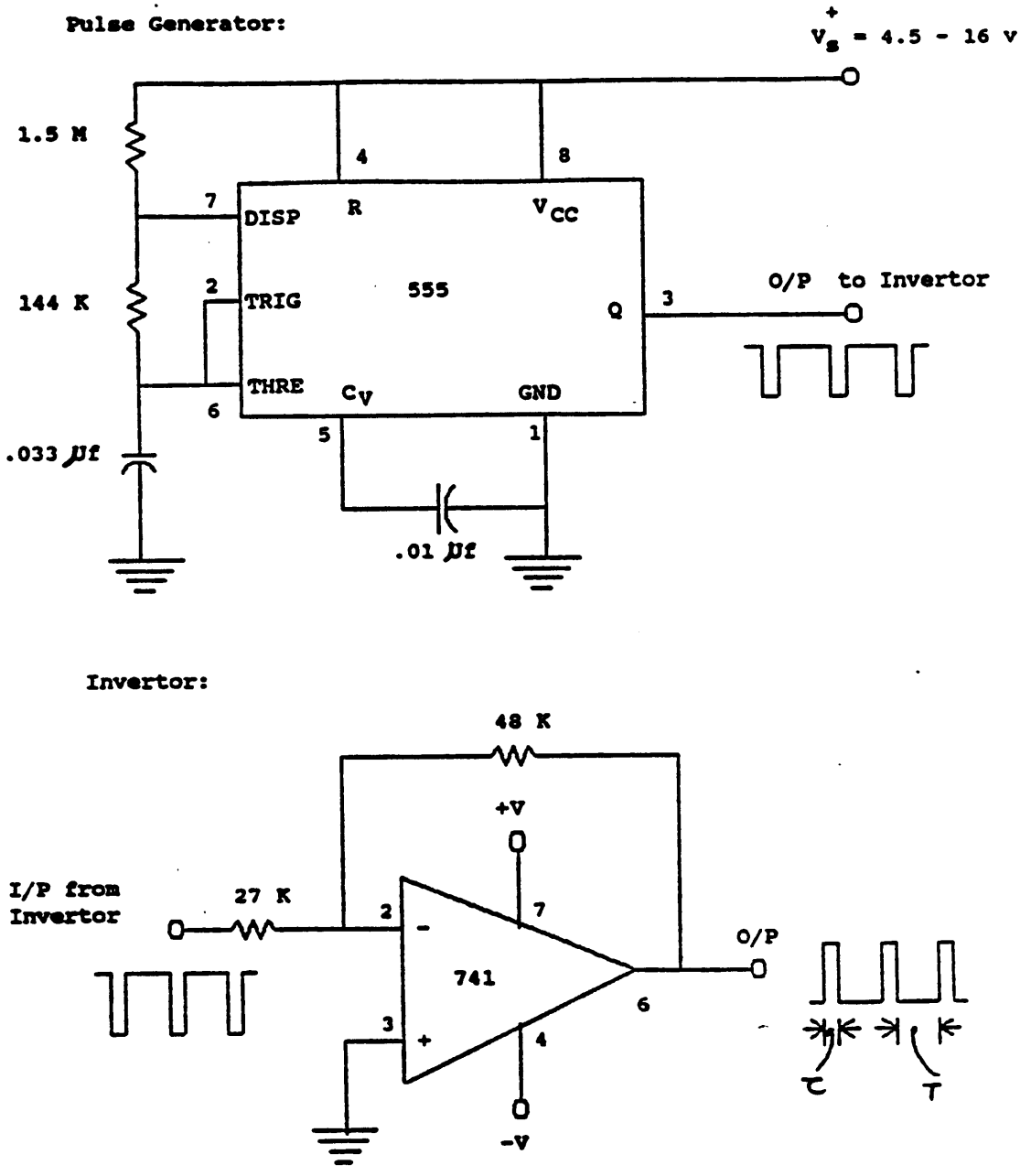

Figure 13. Pulse generator circuit

4.2 1F/FΛ-R hydrophone

The single-fiber, fixed lambda rotational hydrophone was used as the sensing element and experimental results were obtained. The fiber used was plastic clad, 200/250, step index with a numerical aperture 0.6, manufactured by Ensign - Bickford Optics.

Figure 14 shows a typical frequency response curve of the sensor. The response is relatively flat to within a 3 dB range from 15 kHz to 75 kHz. A minimum detectable pressure calculation was carried out based on the transmitting response of the hydrophone and the applied input voltage. This was necessary to quantify the measured pressure because of the lack of another calibrating hydrophone which could be used as a detector. A plot of the minimum detectable pressure versus frequency is shown in Figure 15.

Figure 16 shows oscilloscope traces of the input and output waveforms for a cw operation. Figures 17 and 18 are fast Fourier Transforms (FFT) of the input and output signals, respectively. They prove that the observed output signal is at the same frequency as the applied input signal.

An important performance curve for any practical sensor is its input versus output curve. A characteristic curve, at 45 kHz, is shown in Figure 19. The response is fairly linear. The final application of the sensor is in direction sensing. The variation of output power due to rotation of the sensor by an angle θ was

calculated as follows. At a given input voltage, frequency and distance, the maximum microbend loss was measured when the source was directly in front of the grooves. The sensing element was then rotated and the output at every θ was measured. The loss was than expressed as a fraction of the maximum loss and plotted against θ. This variation, for a pulsed wave operation, is shown in Figure 20.

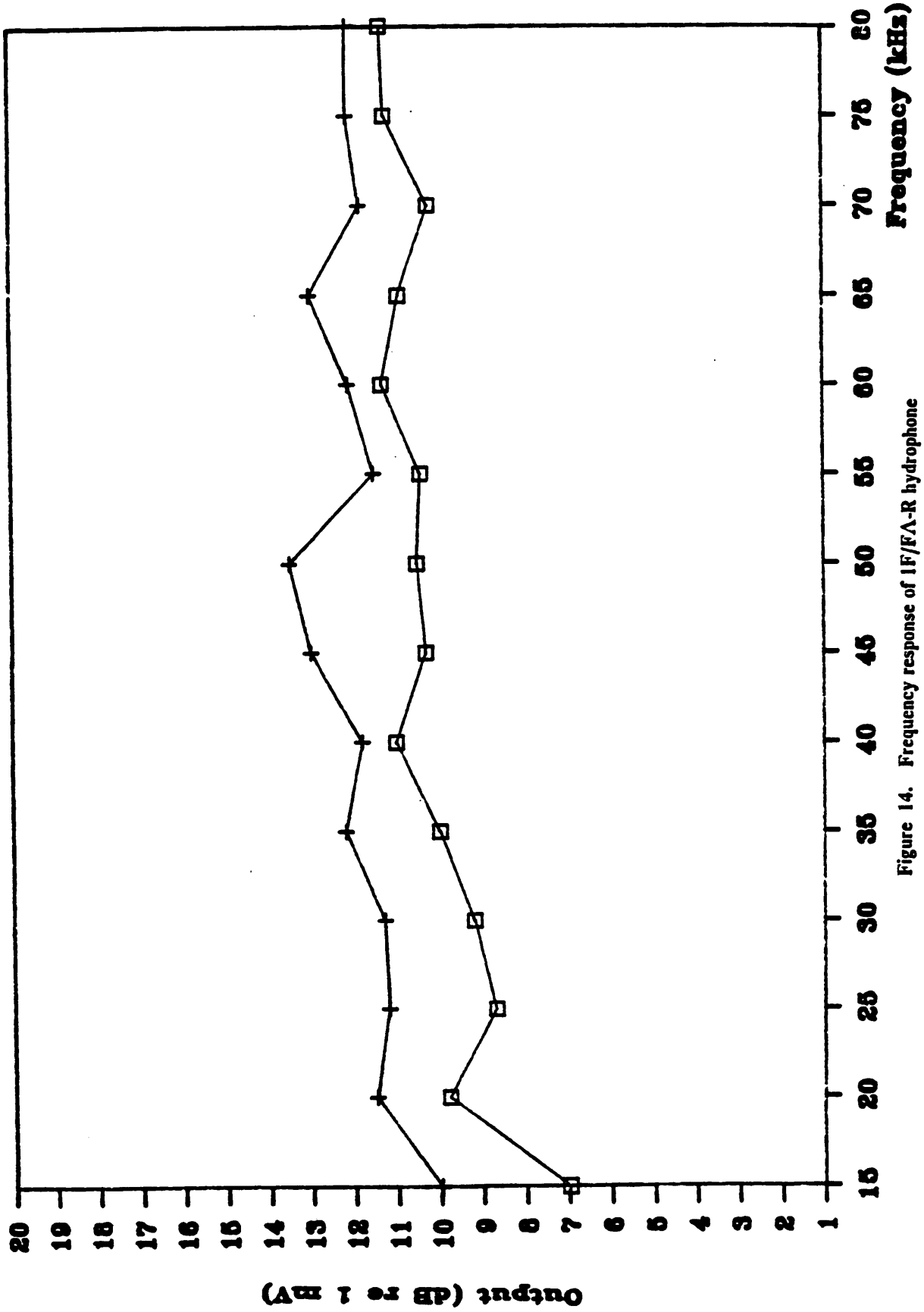

Figure 14. Frequency response of 1F/FA-R hydrophone

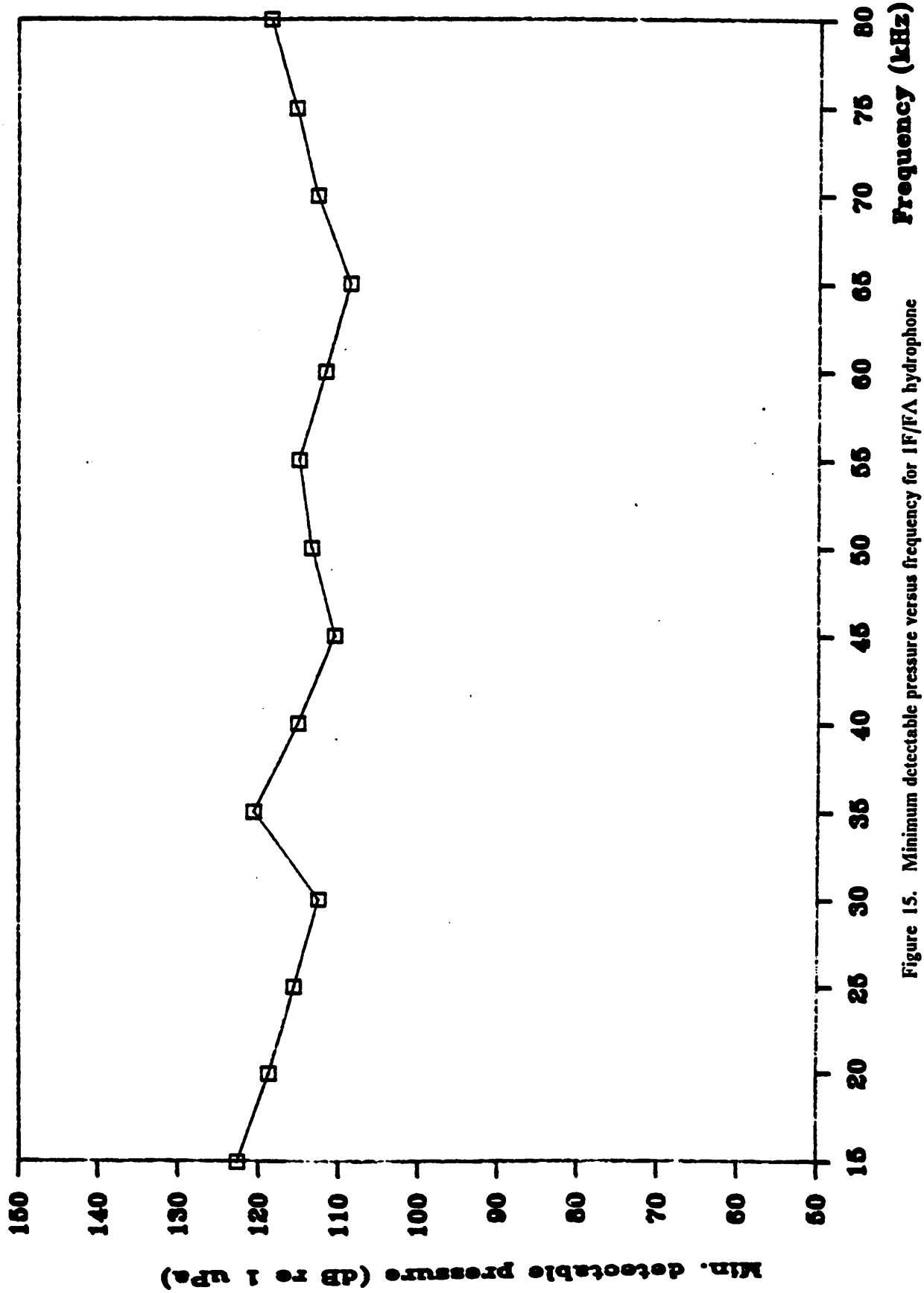

Figure 15. Minimum detectable pressure versus frequency for 1F/FA hydrophone

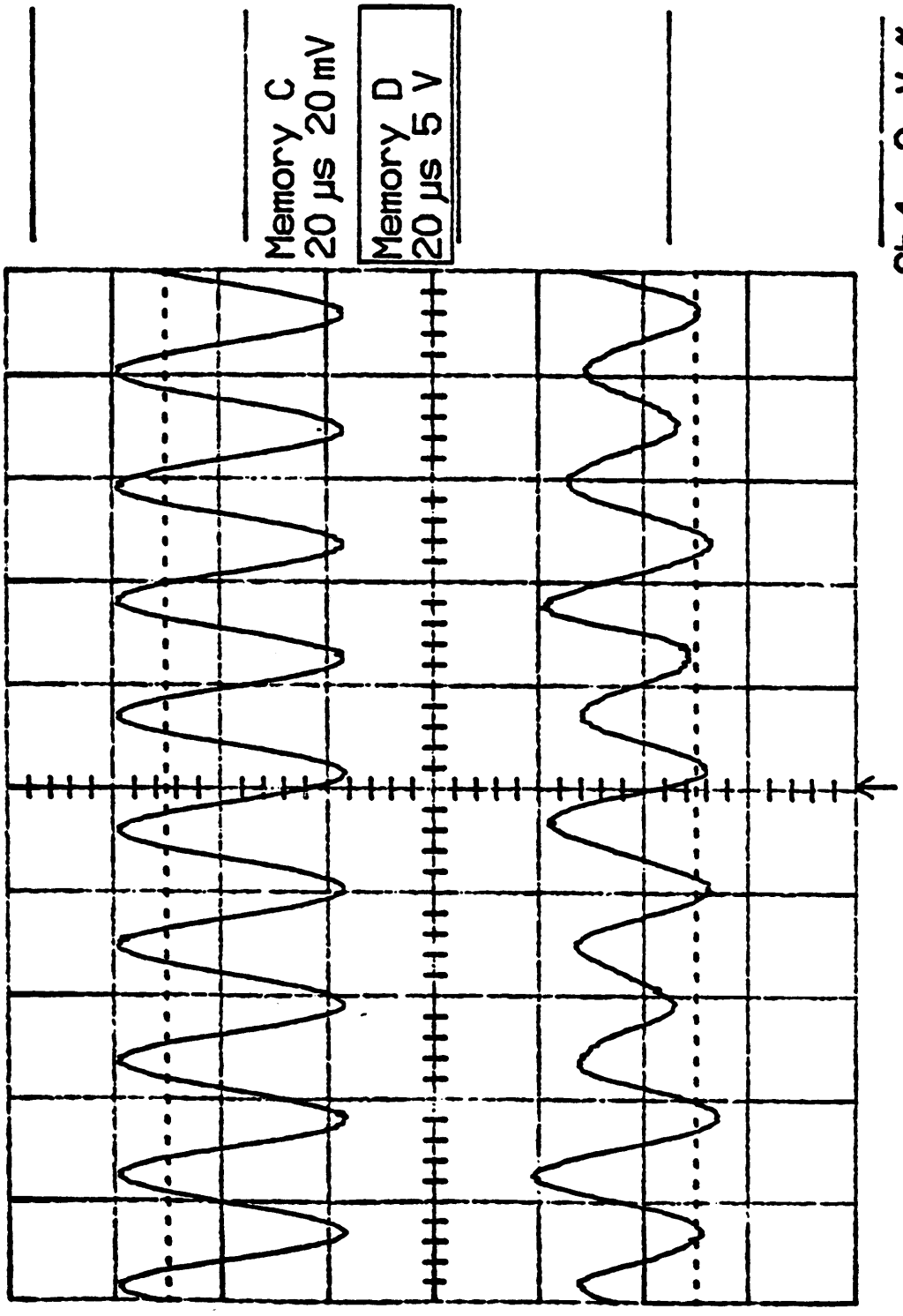

Figure 16. Oscilloscope traces of input and output waveforms for cw operation

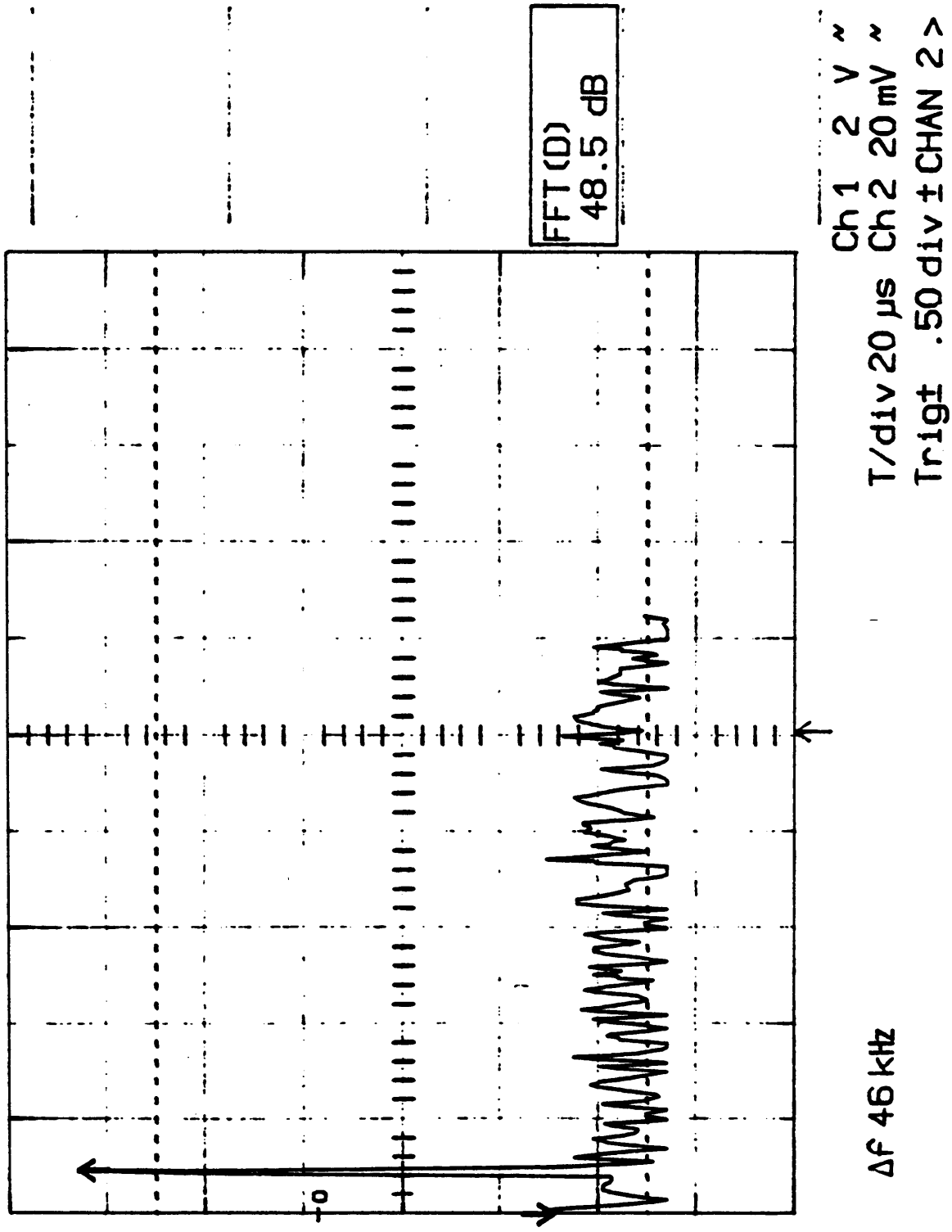

Figure 17. FFT of input waveform in Figure 16

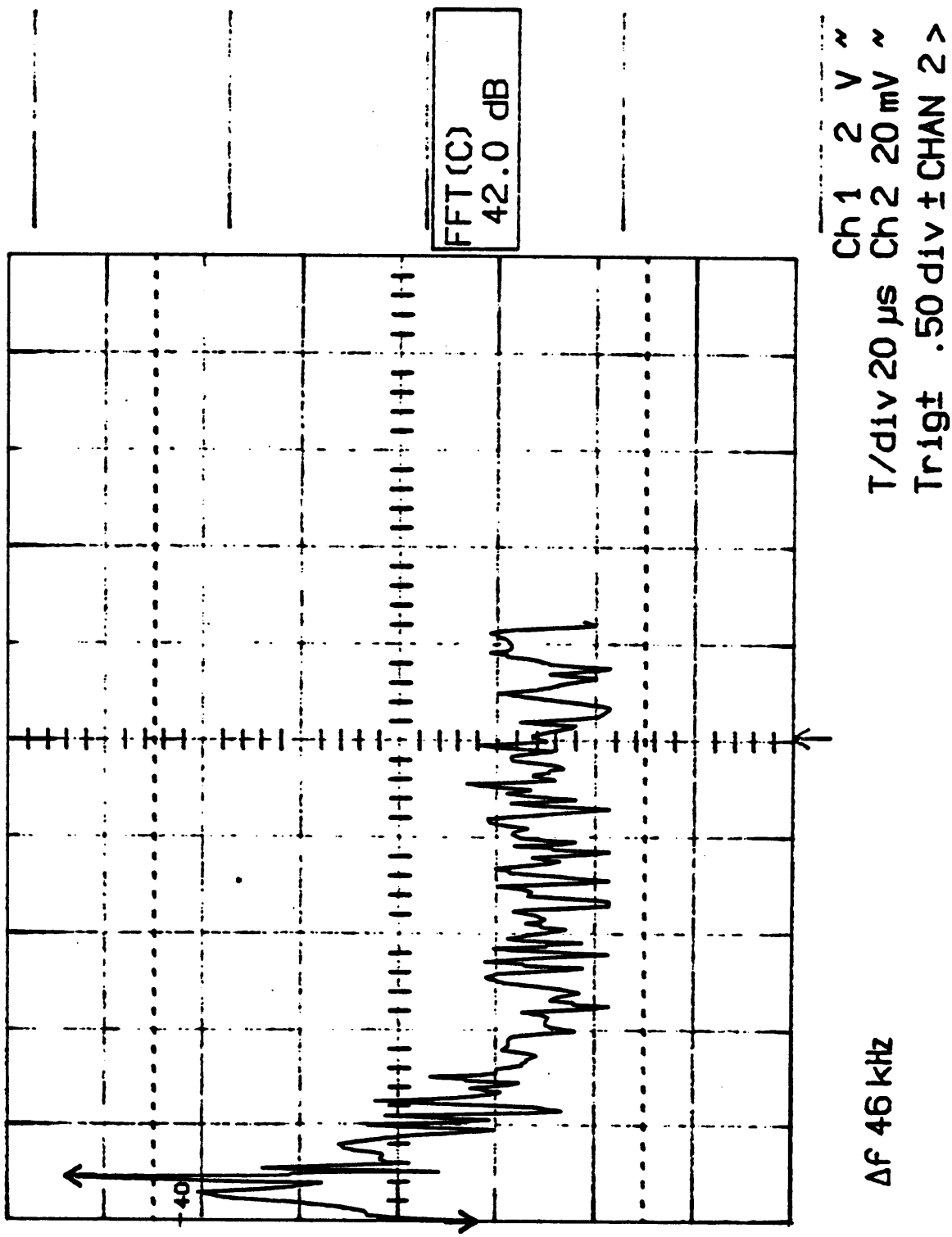

Figure 18. FFT of output waveform in Figure 16

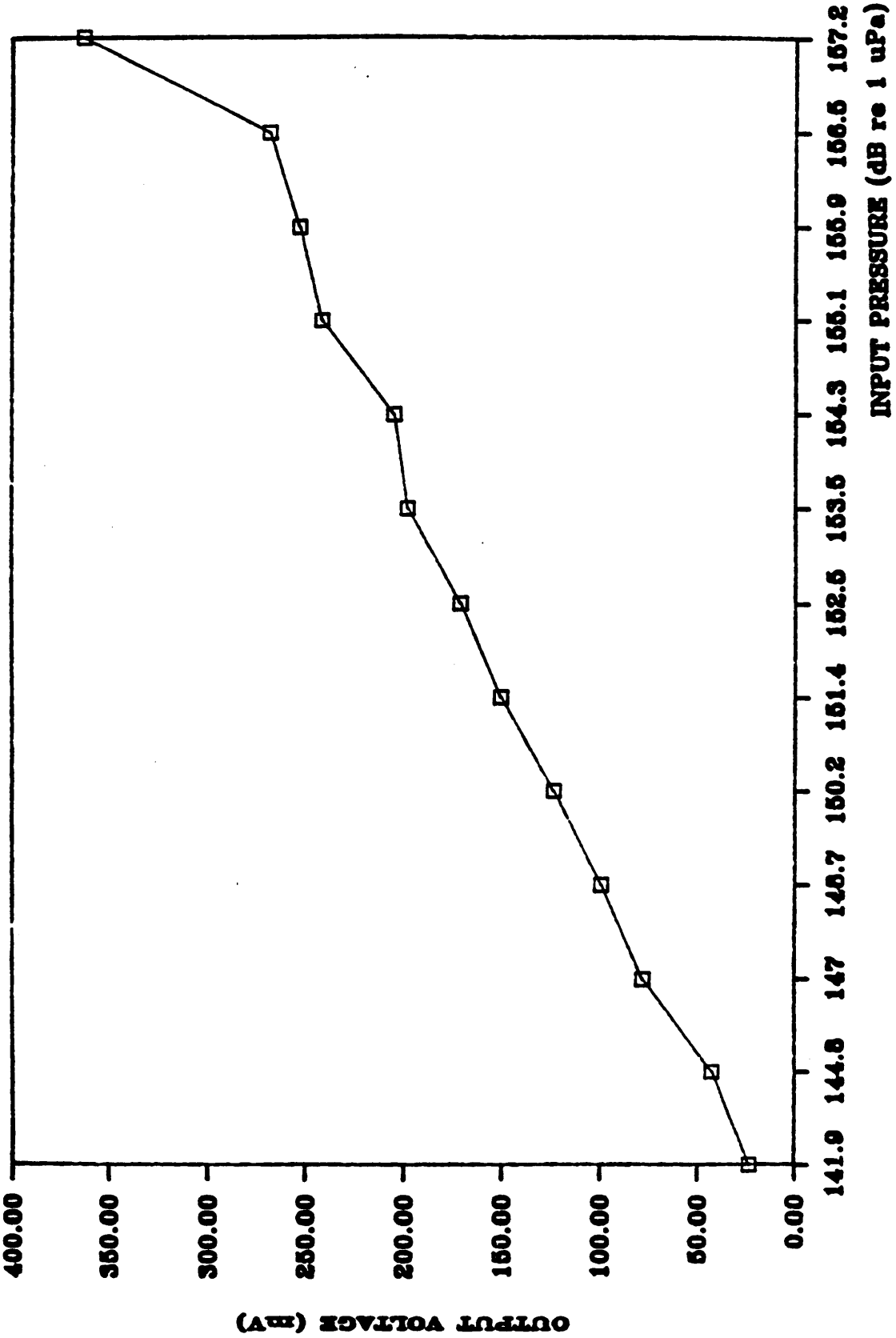

Figure 19. Characteristic input versus output curve for 1F/FA-R hydrophone

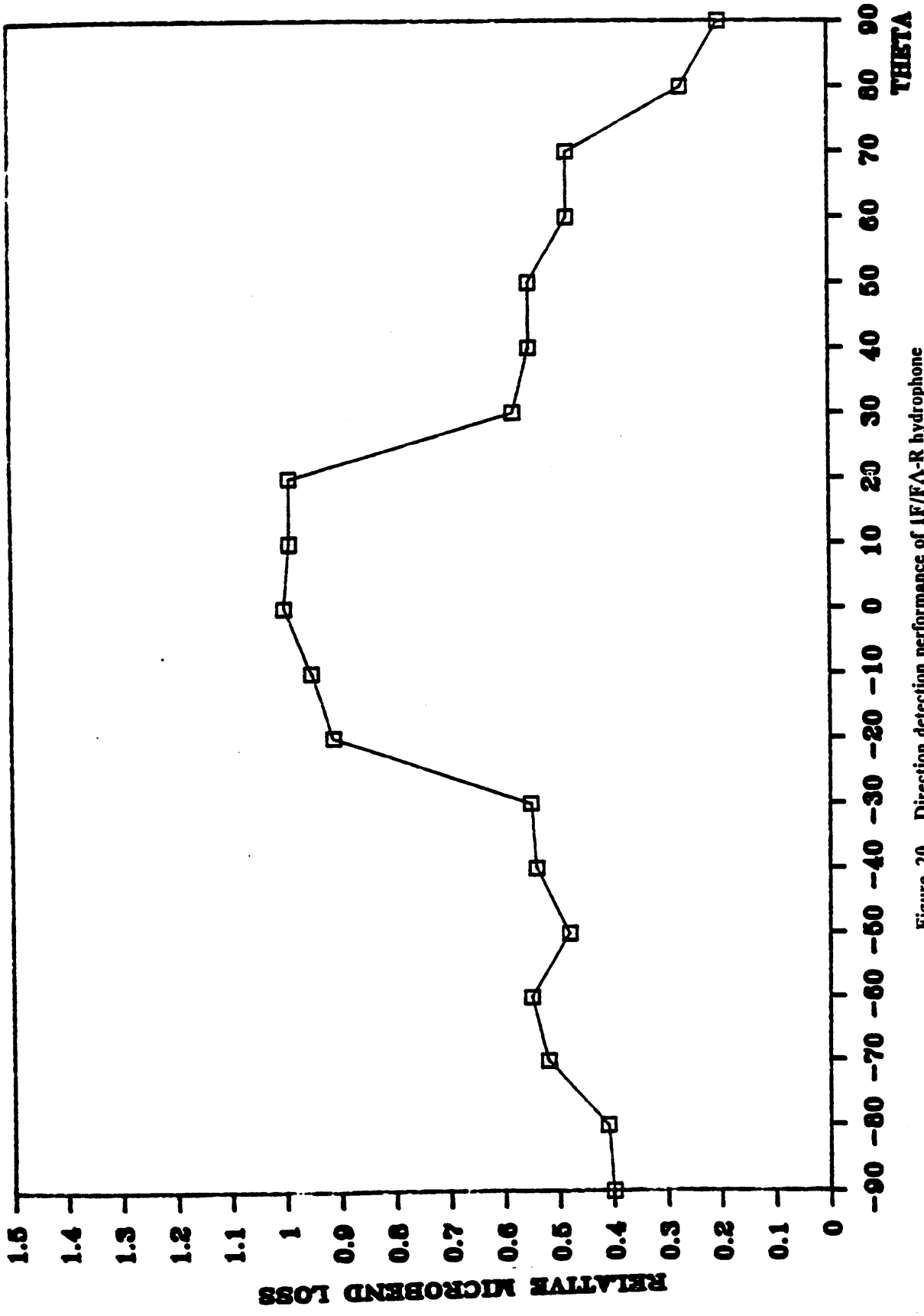

Figure 20. Direction detection performance of 1F/FA-R hydrophone

4.3 3F/FΛ-S hydrophone

The fiber used for the three fiber hydrophone was a parabolic-index, 100/140 with a numerical aperture of 0.2, manufactured by SPECTRAN. A procedure similar to the 1F/F Λ-R hydrophone was followed. Figure 21 shows the comparative outputs, for a pulsed operation, of the three fibers when the source is placed at different angles θ. The detailed graphs of frequency response, input versus output and minimum detectable pressure versus frequency are not given here since the main demonstration of the sensor is for direction detection. Furthermore, amplitude detection and linearity of output has already been demonstrated for the 1F/FΛ case.

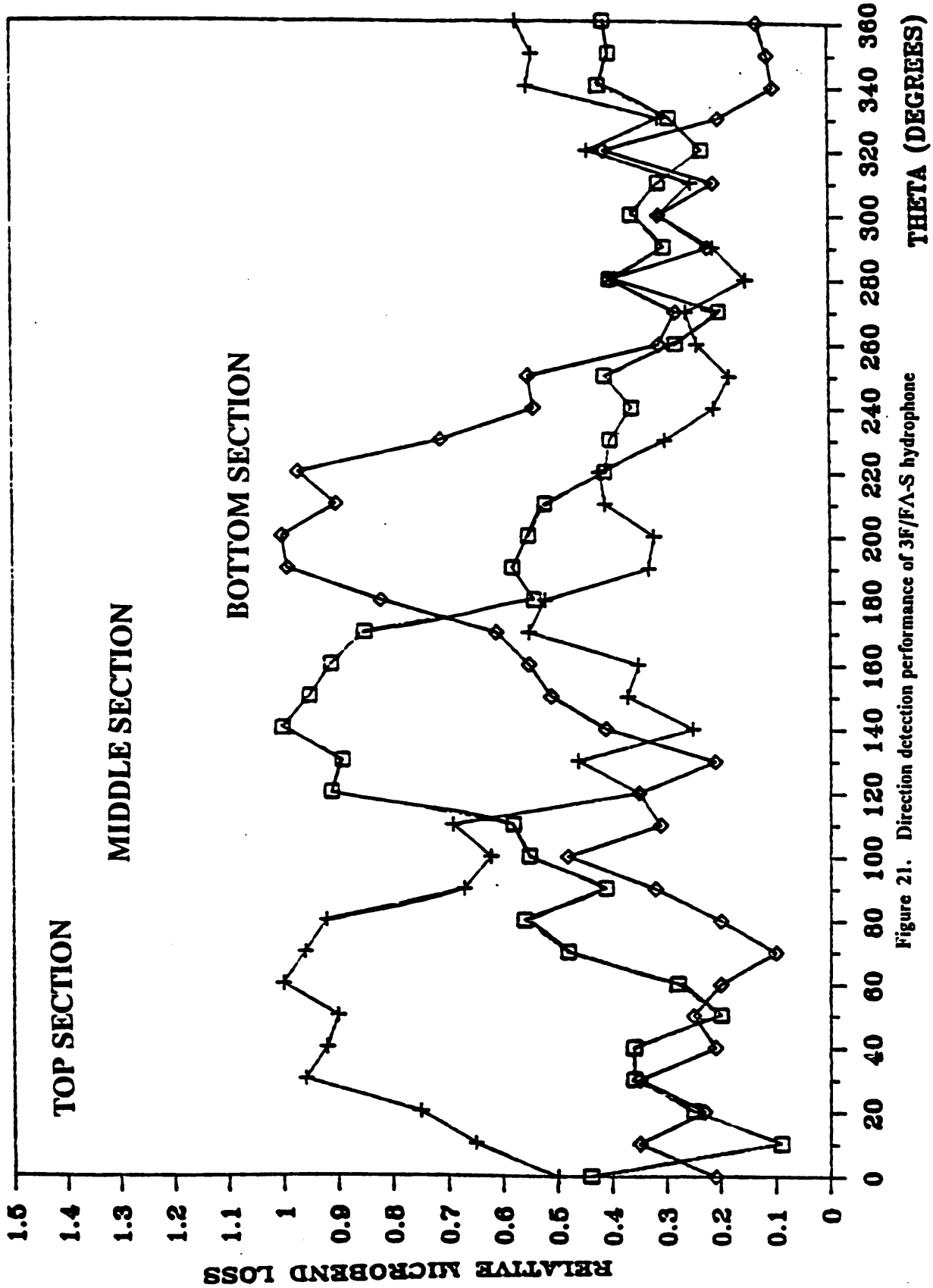

Figure 21. Direction detection performance of 3F/FA-S hydrophone

4.4 1F/VΛ-R hydrophone

The fiber used for the varying lambda hydrophone was step-index, 50/125, numerical aperture 0.18 and manufactured by ITT. Since the mechanical period of perturbation Λ varies along the circumference of the sensing element, the frequency response would be different for different Λs facing the source. Hence, frequency response curves are not shown here. The input versus output curves, for any Λ facing the source,were observed to be as linear as in the 1F/FΛ case. The variation of microbend loss with Λ is given in Figure 22.

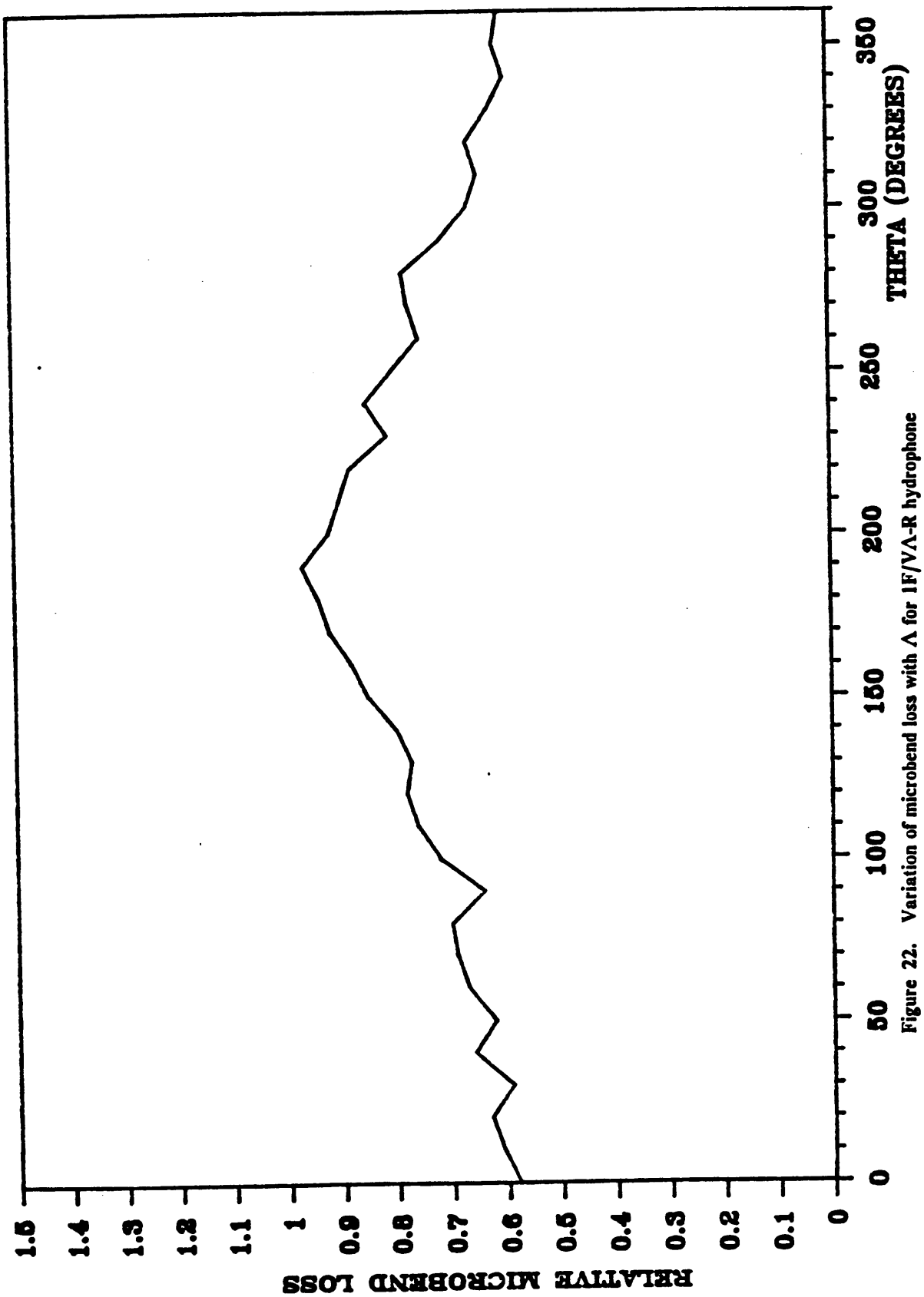

Figure 22. Variation of microbend loss with Λ for 1F/VΛ-R hydrophone

5.0 LAMBDA - DEPENDENT SENSOR PROPOSAL

The design ideas in Chapter 3 suggest, and the experimental results from Chapter 4 highlight, inherent drawbacks associated with the microbend loss multimode fiber optic direction sensors for underwater applications. The two major disadvantages are seen to be:

1. The need for 3 fibers and the simultaneous and comparative monitoring of their outputs as in the 3F/FΛ-S hydrophone and,

2. The need for rotating the sensing element and the dependence of the output on the rotation rate as in the 1F/FΛ-R and the 1F/VΛ-R hydrophones.

An ideal solution to these problems would be a single-fiber sensing element which could be kept stationary. With this in mind, we explore the possibility of using single mode fibers with a wavelength division multiplexing scheme. The theory

summarized in section 2.4 is shown to have potential applications for future research. A well defined proposal is presented. The "proof-of-concept" experiment suggested in this chapter will be the first step in future research.

5.1 Application of Theory

The application of Floquet space harmonics to microbend losses induced in periodic structures has given us an understanding of the variation of such losses with the spatial period Λ, the source wavelength λ and the fiber radius a. As a refresher, Figure 23 shows characteristics of microbend loss in a single-mode fiber plotted against Λ.

It has been proven [21] that the peaked losses observed at λ_1 in Figure 23 result in a step-like behavior of the losses with respect to the source wavelength λ. This step-like variation is shown in Figure 24.

Note that the groove period is chosen as Λ_c. It is also important to note that the peak-like behavior is critically dependent on the fiber radius. It would, however, be true to say that for a given fiber radius one should be able to obtain a peak-like behavior at some λ.

The proposal for future work is based on the assumption that we are able to find two source wavelengths λ_1 and λ_2 over the entire visible and IR range such that microbend loss exhibits the pattern shown in Figure 25.

This, in effect, would imply a microbend loss behavior with respect to source wavelength as shown in Figure 26.

There is no reason to believe that two or more of such wavelengths cannot exist. Theory does not seem to prove otherwise and some of the recent research [22] in the study of wavelength demultiplexing using bends in single-mode fibers has been restricted to a few discrete wavelengths. The use of a newly acquired spectral attenuation measurement system should greatly facilitate research in this area.

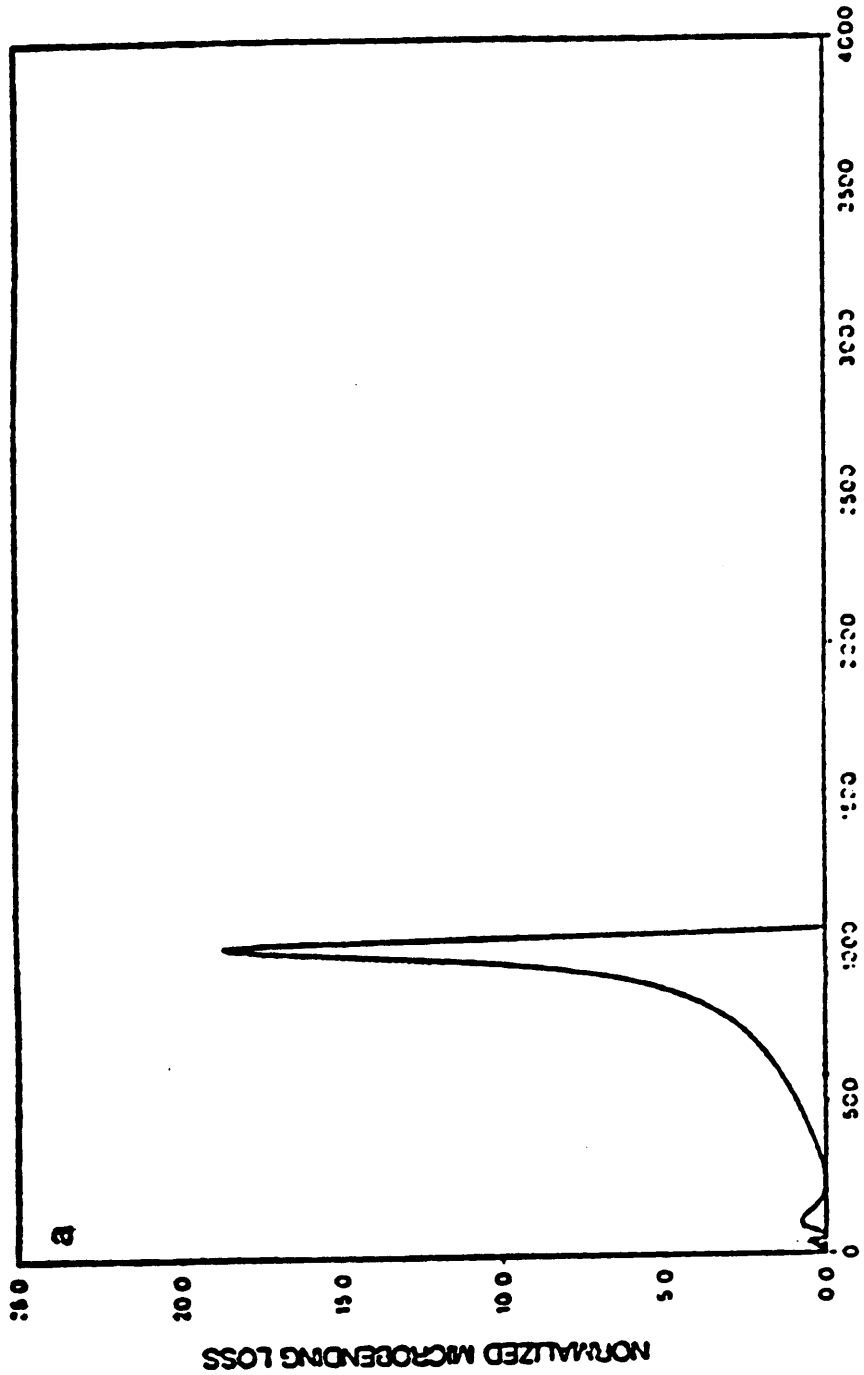

Figure 23. Microbend loss variation with Λ in a single mode fiber [21]

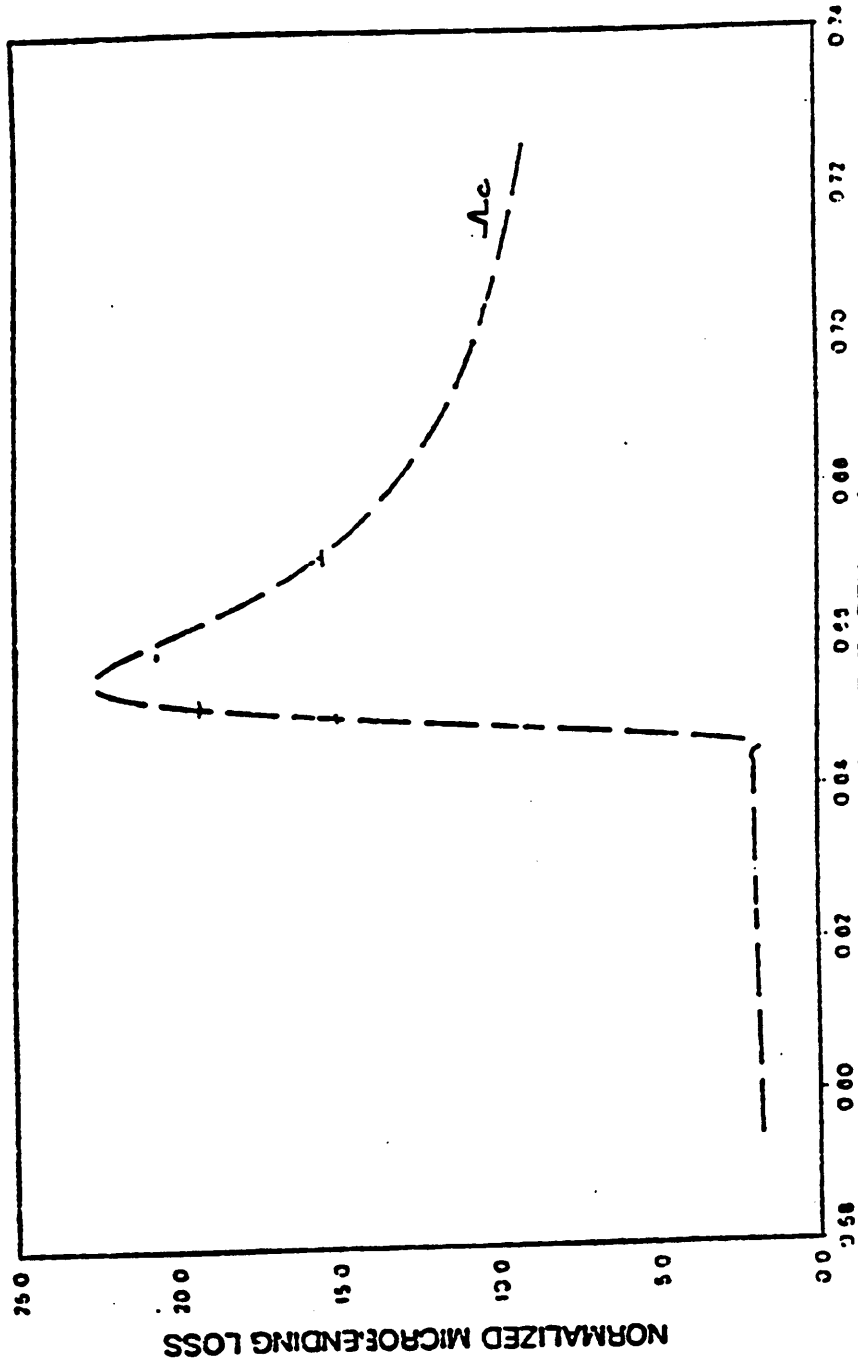

Figure 24. Microbend loss versus λ for a single mode fiber [21]

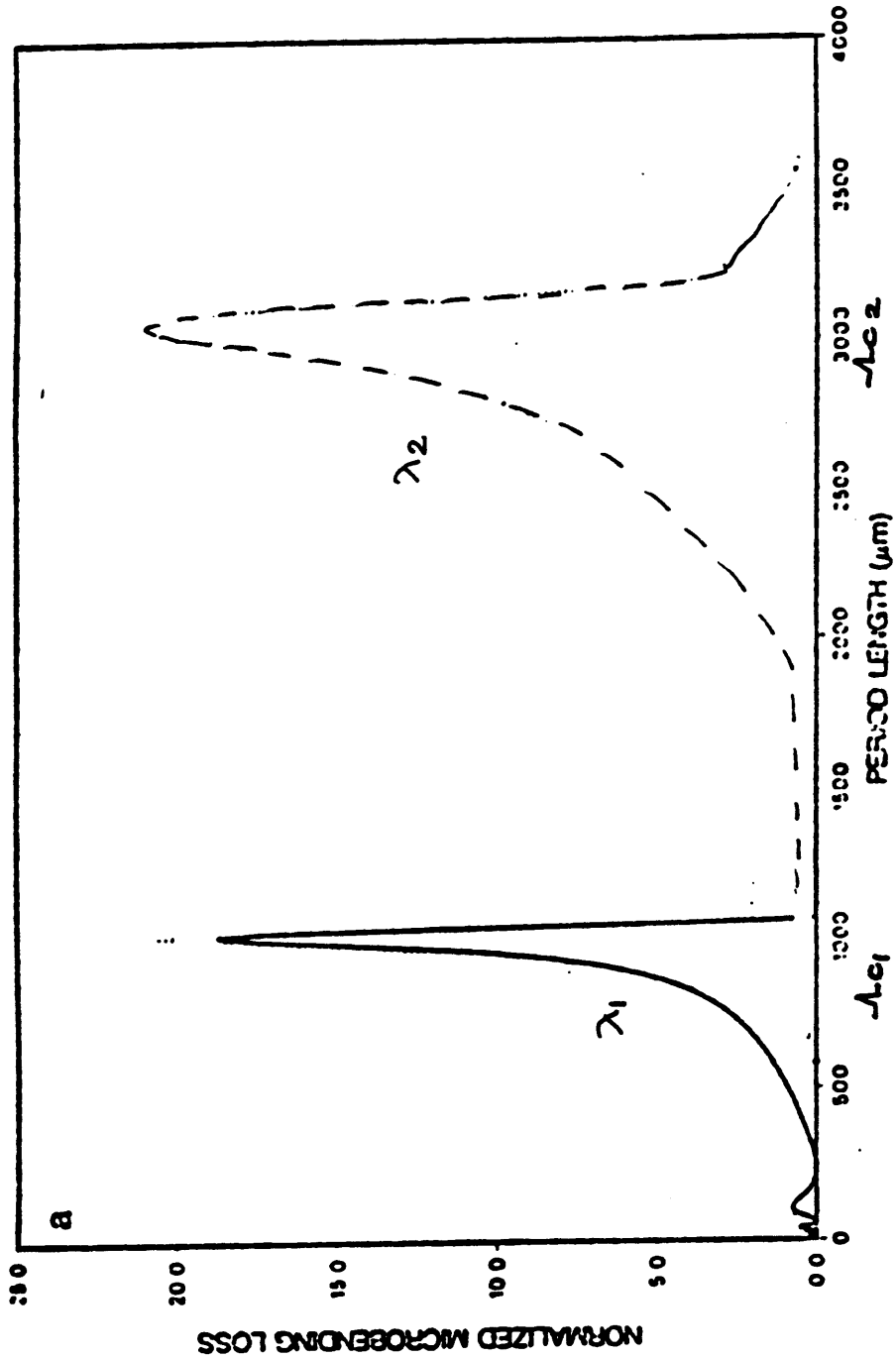

Figure 25. Desired peaked microbend loss behavior at two λs

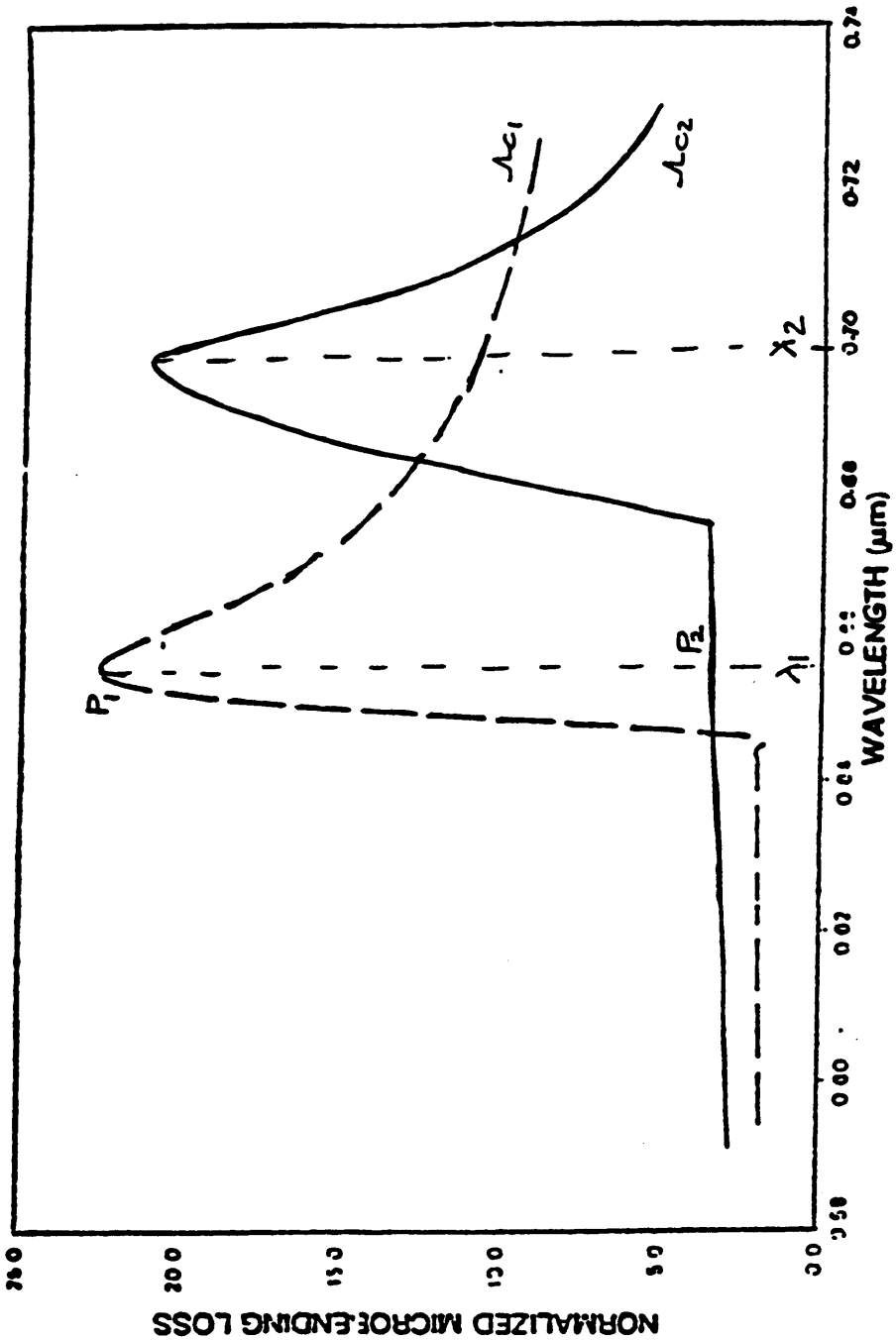

Figure 26. Implication of Figure 25 - microbend loss versus λ

5.2 Proposed Experiments

Based on the previous section a set of systematic experiments are proposed:

1. Choose a large number of fibers with different core radii; the fibers should be single mode at the smallest wavelength λ to be tested.

2. For each fiber, identify one wavelength λ_1 at which the microbend loss exhibits a peak-like behavior. Use the microbend-inducing circular plates that were used in section 3. This would imply an acquisition of a large data base by continuously varying both λ the source wavelength and Λ the spatial period.

3. For every fiber that exhibits the desired behavior at source wavelength λ_1 and spatial period Λ_{c_1} carry out a more microscopic search for a second source wavelength λ_2 with similar microbend loss behavior at a spatial period Λ_{c_2}. A more microscopic search implies varying Λ by a smaller rotation of the grooved plates than in (2) above.

4. Perform a "proof-of-concept " experiment with a cylindrical sensing element as shown in Figure 27.

   The direction sensor would operate on the principle based on Figure 26. Light at wavelengths λ_1 and λ_2 propagates in the fiber and power outputs at

λ_1 and λ_2 are monitored separately at the output. When a pressure wave is incident on region A, as shown in the Figure 27, power in λ_1 would suffer a high loss (indicated by P_1 in Figure 26) where as the power component at λ_2 would suffer a minimal loss (indicated by P_2 in Figure 26). Similarly, when the acoustic wave impinges on region B, powers in λ_1 and λ_2 reverse roles.

5. The above experiment, if successful, will be able to prove the use of two wavelengths for direction sensing. However, to calibrate the sensor one of the problems foreseen is the lack of a power reference. The power content in λ_1 and λ_2 may be too small for use in microbend loss sensors because of the inherent difficulty of launching a broadband light into a single mode fiber. Also in our quest to achieve direction detection we may have lost sensor sensitivity. The following scheme is suggested to counter this problem. Figure 27 shows a single-mode fiber spliced to a multi-mode fiber, both fibers being wrapped around the cylindrical sensing element. The power output P_o which contains the power contributions at all wavelengths, is monitored to calibrate the amplitude of incident wave, the direction of which is determined by P_1 and P_2 . It is important to recall that microbending loss in a multi-mode fiber is independent of the wavelength of light. Hence we are assured that the spliced multi-mode fiber will not change, or harmfully affect, the spectral composition of propagating light.

6. If steps (1) through (5) are successfully executed, a thorough search of all possible combinations of fiber radii, source wavelengths and groove spacings should be carried out. This will lead us to our final goal - an accurate one-fiber, stationary microbend loss fiber optic direction sensor.

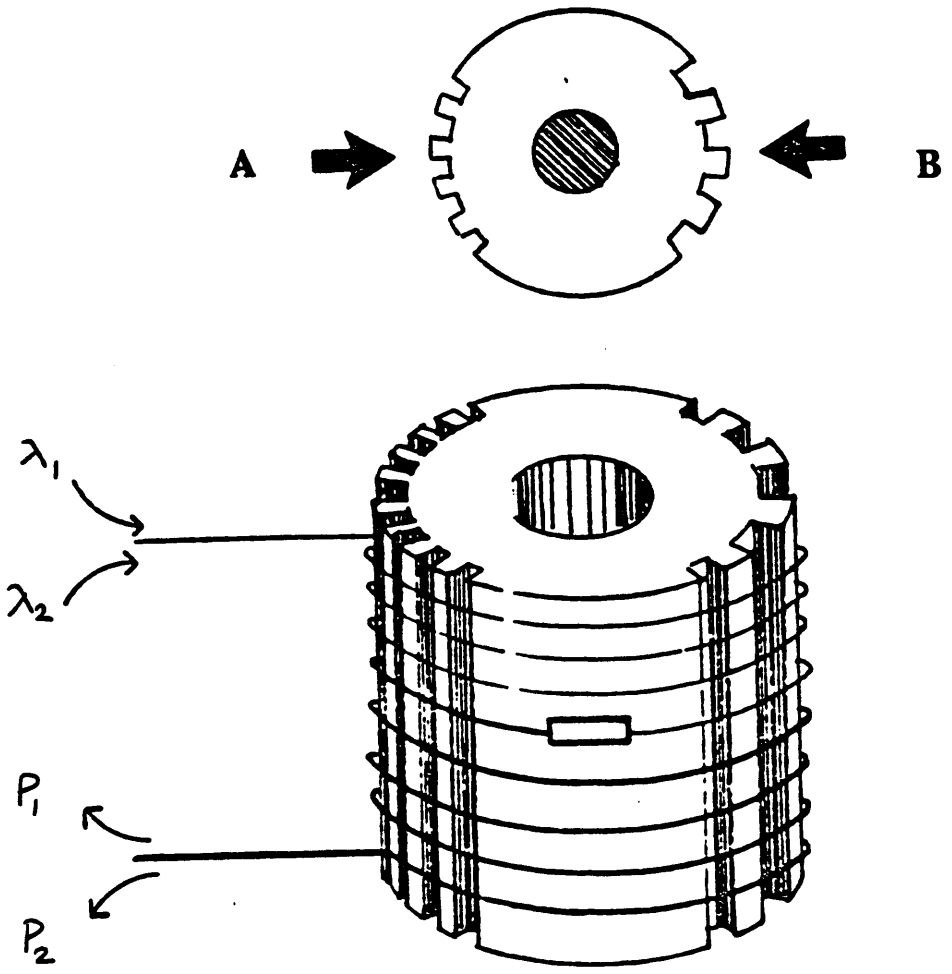

Figure 27. Cylindrical sensing element for use in proposed experiments

6.0 CONCLUSION

The mechanism of microbend loss in multimode fibers has been used to design novel fiber sensors for the detection and measurement of underwater acoustic waves. Three design schemes have been implemented and a comparative analysis has been performed. Based on an experimental study, we have found inherent disadvantages within the design and have proposed a wavelength dependent single mode fiber sensor which should eventually overcome these drawbacks.

Future work should start with a characterisation of different fibers vis a vis the effect of microbend loss at various mechanical wavelengths of perturbation. Efforts should be made to stabilize the optical outputs obtained when the sensor is placed under water. It is also important to use another piezo-electric hydrophone as a sensor for exact experimental verification of the pressure being measured.

It is hoped that the experiments will verify the theoretical results and the ultimate goal of a stationary single-fiber direction cum amplitude sensor for underwater acoustic sources will be achieved.

References

1. Culshaw B., Optical Fiber Sensing and Signal Processing , Peter Peregrinus, London, 1984.

2. Giallorenzi T.G., Bucaro J.A., Dandridge A., Sigel G.H., Cole J.H., Rashleigh S.C., and Priest R.C., "Optical Fiber Sensor Technology " , IEEE Journ. Quant. Elect., v QE-18, pp. 626-652, 1982.

3. Lagakos N., Trott W.J., Hickman T.R., Cole J.H., and Bucaro J.A., "Microbend Fiber Optic Sensor as Extended Hydrophone" IEEE Journ. Quant. Elect., v QE-18, pp. 1633-1638, 1982.

4. Fields J.N., Asawa C.K., Ramer O.G., and Barnowski M.K., "Fiber Optic Sensor", Journ. Acoust. Soc. Amer., v 67, pp. 816-818, 1980.

5. Fields J.N., Asawa C.K., Smith C.P., and Morrison R.J., "Fiber Optic Hydrophone", in Physics of Fibers , v 2, Advances in Ceramics , Bendow B., and Mitra S., Eds. American Ceramic Society, pp. 529-538, 1981.

6. Lagakos N., Litovitz T., Macedo P., Mohr R., and Meister R.," Multimode Optical Fiber Displacement Sensor", App. Opt., v 20, pp. 167-168, 1981.

7. Yariv A., Introduction to Optical Electronics , Holt Reinhart and Winston, New York, 1971.

8. Gloge D., "Optical Power Flow in Multimode Fibers", Bell Sys. Tech. Journ., v 51, pp. 1767-1783, 1972.

9. Marcuse D., Theory of Dielectric Optical Waveguides , Academic Press, New York, 1974.

10. Gloge D., and Marcatili E.A.J., "Multimode Theory of Graded Core Fibers", Bell Sys. Tech. Journ., v 52, pp. 1563-1578, 1973.

11. Kurtz C.N., and Streifer W., "Guided Waves in Inhomogenous Focusing Media Part II: Asymptotic Solution for General Weak Inhomogeneity",IEEE Trans. Microwave Thy. & Tech., v MTT-17, pp.250-263, 1969.

12. Singer F.L., Strength of Materials , Harper and Brothers, New York, 1962.

13. Marcuse D., "Microbending Losses of Single Mode, Step-Index and Multimode Parabolic-Index Fibers", Bell Sys. Tech. Journ., v 55, pp. 937-955, 1976.

14. Peterman K., "Microbending Losses in Monomode Fibers", Electron. Lett., v 12, pp. 107-109, 1976.

15. Taylor H.F., "Bending Effects in Optical Fibers", Journ. Lightwave Tech., v LT-2, pp. 617-628, 1984.

16. Sakai J., "Microbending Loss Evaluation in Arbitrary Index Single Mode Optical Fibers. Part I: Formulation and General Properties ", IEEE Journ. Quant. Elect., v QE-16, pp. 36-44, 1980.

17. Gambling W.A., Matsumura H., and Ragdale C.M., "Curvature and Microbending Losses in Single Mode Optical Fibers", Opt. & Quant. Elect., v 11, pp. 43-59, 1979.

18. Nayfeh A.H., Perturbation Methods , Wiley, New York, pp. 228-240, 1973.

19. Wlodarczyk M.T., and Seshadri S.R.,"Radiation from a Periodically Bent Cylinder with a Graded-Index Profile", Journ. Lightwave Tech., v LT-3, pp. 713-724, 1985.

20. Wlodarczyk M.T., and Seshadri S.R., "Radiation losses in a Periodically Deformed Single-Mode Fiber", Journ. Lightwave Tech., v LT-5, pp. 163-173, 1987.

21. Wlodarczyk M.T., "Wavelength Referencing in Single-Mode Microbend Sensors", Opt. Lett., v 12, pp. 741-743, 1987.

22. Harris A.J., Shrubshall P.A., and Castle P.F., "Wavelength Demultiplexing using Bends in a Single Mode Optical Fiber ", Journ. Lightwave Tech., v LT-6, pp. 80-86, 1988.

The vita has been removed from the scanned document